The Caretaker Role of ARID1A in DNA Repair and
the Effects of Targeted Therapy in ARID1A Mutated Cancers

by
Youngran Park

A dissertation submitted to Johns Hopkins University in conformity

with the requirements for the degree of Doctor of Philosophy

Baltimore, Maryland

September, 2017

Abstract

Somatic inactivating mutations in *ARID1A*, a component of the SWI/SNF chromatin remodeling complex, have been identified in various human malignancies, and are particularly common in tumors originating from endometrial epithelium (i.e. endometrioid adenocarcinoma of the uterus and endometriosis-associated ovarian cancers). Loss of ARID1A compromises DNA damage repair *in vitro*, but the underlying mechanisms and clinical relevance of these findings are unclear.

In the present study, we observed increased DNA damage in association with ARID1A-deficiency in endometrial tissues from human samples and from an inducible PAX8-driven *Arid1a*-deletion mouse model. Using isogenic pairs of cell lines differing only in ARID1A status, we demonstrate the indispensable role of ARID1A in establishing an open chromatin state at DNA double strand breaks, which is necessary for the repair proteins 53BP1 and RIF1, components of the non-homologous end-joining (NHEJ) machinery, to access and repair the damage. The inability of ARID1A$^{-/-}$ cells to mount an NHEJ-mediated DNA repair response renders them more sensitive to irradiation than ARID1A intact controls. Small-molecule compound screens conducted in isogenic cell lines revealed that the PARP inhibitor, Olaparib, synergizes with radiation to elicit cytotoxicity selectively in the context of ARID1A deficiency. Combination treatment with low-dose radiation and Olaparib demonstrated improved efficacy in reducing tumor growth in mouse xenograft models of *ARID1A*-mutant endometrial and ovarian clear cell carcinomas compared to either treatment alone, while no improvements over monotherapy

were observed in mice carrying *ARID1A* intact tumors. Since ARID1A functions in a "caretaker" role by facilitating NHEJ-mediated repair of DNA DSBs, inducing a high burden of DSBs, by combining radiation with PARP inhibition, may be a particularly efficacious strategy for the treatment of ARID1A deficient gynecologic cancers.

Readers:

Ie-Ming Shih, M.D., Ph.D.

Tian-Li Wang, Ph.D.

Thesis Committee Members:

Sonia Franco, MD., Ph.D

Anthony K. L. Leung, Ph.D.

Ie-Ming Shih, M.D., Ph.D.

Tian-Li Wang, Ph.D.

Thesis Advisor:

Ie-Ming Shih, M.D., Ph.D.

Tian-Li Wang, Ph.D.

Acknowledgments

I owe the majority of my scientific and personal growth over the past six years to my mentors, friends, family, and to the coworkers and classmates that I have been lucky enough to meet here at Johns Hopkins.

First and foremost, I would like to express my sincerest gratitude to my advisors, Dr. Ie-Ming Shih and Dr. Tian-Li Wang. Drs. Shih and Wang are diligent, passionate sharp scientists and great mentors whom I respect and look up to a great deal. Despite their myriad of other responsibilities, Drs. Shih and Wang have selflessly invested so much of their time and energy in my academic development. They always made themselves available whenever I had questions or needed their guidance. It has been a great privilege to work with them over the last five years.

Next, I would next like to thank the other members of my thesis advisory committee, Drs. Sonia Franco and Anthony K. L. Leung, for generously contributing their time and intellectual guidance along the way. They have provided invaluable input as well as useful reagents for my project without any hesitation.

I would like to thank all the past and current members of the "Shih/Wang" lab, who have created a workplace that is educational, fun, and supportive. Especially to Yohan, Asli, Jin, Sherine, Yuyu and Ayse for their great friendship and encouragement whenever I feel frustrated. I also thank Herman, Tiffany and Karime for their kindness to read and edit my thesis. Also, I appreciate Wenjing, Tsutomu, and Ryoichi who were involved in generating and maintaining our mouse model. Without help from Michael, Marina, Esteban,

Table of Contents

List of Tables

List of Figures

For Taesuh

Chapter 1. Introduction

1-1. Gynecologic Cancer and Its Heterogeneity

Gynecologic cancer is a heterogeneous family of neoplasms with different histopathologic and molecular genetic features. Among them, ovarian cancer is the leading cause of gynecologic cancer deaths in the world although it is not the most common cancer of the female reproductive system.[1,2] For many decades, extensive research provided valuable insights into the origin and molecular pathogenesis of ovarian cancer and currently, a dualistic model of epithelial ovarian carcinogenesis is widely accepted.[3] According to this model, ovarian cancer is divided into two groups; type I and type II. Type I tumors include endometriosis-related tumors such as endometrioid, clear cell, and seromucinous carcinomas. It also includes low-grade serous carcinomas (LGSC), mucinous carcinomas and malignant Brenner tumors. Type I tumors are believed to originate from extra-ovarian lesions such as endometrial epithelium that implanted on the ovary. High-grade serous carcinomas (HGSC), on the other hand, are classified as type II tumors and derive from the fallopian tube end and disseminate into the ovary.[3]

Each histologic subtype is associated with distinct genetic signatures (**Table 1-1**). In ovarian HGSC, the most frequent genetic alteration found is the TP53 mutation (>80% of cases).[4,5] In addition to TP53 mutation, CCNE1 (encoding cyclin E1) amplification, BRCA1and BRCA2 mutation are commonly found in HGSC. In contrast to HGSC, TP53 mutations are uncommon (8%) in low-grade serous carcinoma.[5] However, KRAS or BRAF mutations have been commonly observed in LGSC. Mucinous carcinomas present KRAS mutations in more than 50% of specimens.[6] Ovarian clear cell (OCCC) and endometrioid carcinomas, unlike other subtypes, share similar genetic alterations, and data suggest that

those cancers are derived from endometriosis.[7-10] ARID1A and PIK3CA are frequently mutated in those cancers. More than half of endometriosis-related ovarian carcinomas present ARID1A loss, suggesting that ARID1A loss plays an important role in these cancers.[11-14]

Not only genetic signatures but also clinical behaviors, especially in response to standard chemotherapy, differ according to histologic subtype (**Table 1-2**). The standard therapy for ovarian cancer is primary debulking surgery (PDS) followed by platinum and taxane chemotherapy. HGSC, the most common subtype (70%), is highly responsive to this treatment. However, 80% of patients with advanced stage HGSC develop disease recurrence.[15,16] In contrast, LGSC and OCCC are intrinsically resistant to the standard therapy. Particularly, OCCC, the second most common ovarian epithelial cancer, has posed challenges for clinicians and scientists for being associated with poor prognosis even when diagnosed at early stages.[17]

Endometrial carcinoma (EC) is the most prevalent gynecological cancer and the fourth most common malignant neoplasm among women in the United States.[18] Similar to ovarian cancer, EC is also classified based on epidemiological and clinical findings.[19] Type I EC is estrogen-dependent and develop from endometrial hyperplasia. However, type II EC is estrogen-independent and arise in atrophic endometrium or in endometrial polyps. Histologically, type I carcinomas are generally of endometrioid subtype, and type II is composed mainly of serous carcinoma, which resembles ovarian HGSC histologically and clinically. Similar to those in ovarian cancer, each subtype of EC also has unique genetic

signatures. Genetic mutations in ARID1A and PI3K pathway-related genes are common in type I tumors, whereas TP53 mutations are associated with type II EC.[20,21]

Despite such a considerable difference between subtypes, ovarian and endometrial cancer has historically been treated as one entity. This can be one of the reasons why prognosis of gynecologic cancer has barely changed in the last 30 years. Hence, understanding the distinctive mechanisms of each subtype is necessary to provide guidance on personalized treatment. Furthermore, based on the genetic alteration, development of new therapeutic strategies is the most urgent issue for improving prognosis. In this thesis research, we set out to study the function of ARID1A, the most frequently mutated gene in OCCC and uterine endometrioid carcinoma. Specifically, we intend to reveal the role of ARID1A during the DNA double-strand repair process. In addition, based on our discovery, we propose a personalized therapy to cure patients with ARID1A mutations.

Ovarian Epithelial Cancer				
HGSC	LGSC	Mucinous	Clear cell	Endometrioid
TR53	BRAF	KRAS	ARID1A	ARID1A
BRCA1/2	KAS	HER2 amp	PIK3CA	PIK3CA
NF1	NRAS		PTEN	PTEN
RB1	ERBB2		CTNNB1	CPPP2R1a
CDK12			CPPP2R1a	MMR defects
HR defects				

Table 1-1. Histologic subtypes of ovarian cancer and associated molecular aberrations. (modified from reference [22])

	HGSC	Endometrioid	Clear cell	Mucinous	LGSC
Approximate proportion of OC cases	70%	10%	10%	< 5%	< 5%
Tissue of origin/ precursor lesion	Distal fallopian epithelium	Endometriosis	Endometriosis	Poorly defined	Serous borderline tumor
Intrinsic chemosensitivity	High	High	Low	Low	Low

Table 1-2. Characteristic of the five main histological subtypes of ovarian cancer (modified from reference [23])

1-2. The Significance of ARID1A Mutation in Gynecological Cancer

ARID1A is a member of the SWItch/Sucrose NonFermentable (SWI/SNF) chromatin remodeling complex which is originally found in yeast genetic screening.[24,25] The SWI/SNF complex remodels chromatin structure and is capable of mobilizing nucleosomes by utilizing the energy of ATP hydroxylation. They slide and catalyze the ejection and exchange of histone octamers depending on the condition.[26] This process tightly regulates critical processes such as transcription, DNA replication, methylation and DNA repair.[27] As this regulation is one of the most crucial parts of the cellular process, dysregulation of ATP-dependent SWI/SNF complex leads to severe problems such as cancer. Recently, many researchers found that more than 20% of all human cancers have mutations in the SWI/SNF complex and this suggests the importance of SWI/SNF in genomic integrity.[28,29]

The gene that encodes ARID1A, a subunit of SWI/SNF complex, is the most frequently mutated gene in endometriosis-associated gynecologic cancers including OCCC (46–57%) and EC (39-44%).[11,12,30] (**Figure 1-1**). Subsequent comprehensive sequencing efforts have reported frequent somatic mutations in *ARID1A* in other types of cancers including gastric carcinoma (8~29%),[31-34] esophageal adenocarcinoma (9~19%),[35-37] Waldenstrom's macroglobulinemia (17%),[38,39] pediatric Burkitt lymphoma (17%),[40] hepatocellular carcinoma (10~16%),[41,42] cholangiocarcinoma (14~15%),[43,44] and urothelial carcinoma of bladder (12~15%).[45-47] Since the majority of ARID1A somatic mutations are nonsense or frameshift types, leading to loss of expression and inactivation, the biological consequence of *ARID1A* mutations is the loss of function.[48]

In *in vitro* cell model, silencing of ARID1A expression increases cellular proliferation, while induced ARID1A expression in *ARID1A* mutated ovarian clear cell carcinoma cells inhibits cell growth and suppresses tumorigenicity.[48] In genetically engineered mice, *ARID1A* deletion in combination with *PTEN* inactivation or PIK3CA activation in the ovarian surface epithelium is sufficient to promote the development of ovarian endometrioid or clear cell-like tumors.[49] Collectively, these reports indicate a potential cooperation of ARID1A deletion with the PI3K/AKT pathway activation in promoting cancer developmentc and explain the high frequency of co-mutation of *ARID1A* and PI3K/AKT pathway-related genes in human cancer.[50 51]

Partly due to pleiotropic function and difficulty in studying a nuclear complex with more than 10 subunits, detailed mechanisms underlying the tumor suppressor functions of ARID1A remain largely unclear. We have previously shown that ARID1A participates in the transcriptional regulation of p53-dependent genes including *CDKN1A*,[52] and thus ARID1A assumes a "gatekeeper" role in preventing cellular proliferation. On the other hand, the somatic mutation at h*TERT* promoter that activates TERT transcription tends to be mutually exclusive with ARID1A inactivation.[53] Functional inactivation of ARID1A enhances TERT transcription and maintains telomere length in cancer cells,[54] indicating that ARID1A also participates in regulating telomere length and guards genomic integrity, so it can also be considered as a "caretaker".
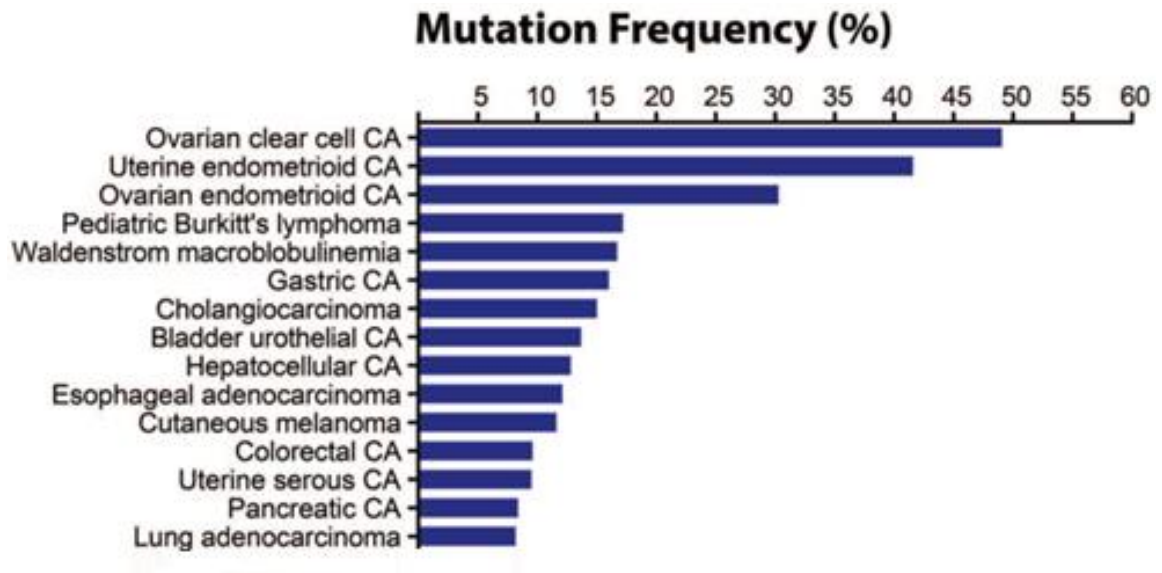
Figure 1-1. Top 15 human cancers with most frequent mutation with ARID1A. (modified from reference [30]) A total of 594 mutated samples from 5160 tumors belonging to 25 different tumor types have been reported.

1-3. The Role of ARID1A in Maintaining Genomic Integrity of Gynecologic Cancer

The maintenance of genome integrity is pivotal for cell survival, homeostasis and transferring genetic material to the next generation. However, there are numerous endogenous cellular events and exogenous environmental agents that compromise genomic integrity throughout the lifespan. To protect genetic information from these deleterious events, cells have been evolutionally developed sophisticated DNA repair systems. Depending on the type of the damage, repair systems can be classified as DNA single strand breaks (SSB) repair and DNA double strand breaks (DSB) repair, which can further be divided into homologous repair (HR) and non-homologous end joining (NHEJ).

SSB repair deals with damage when only one DNA strand is damaged. SSBs are commonly generated by endogenous reactive oxygen species (ROS) during normal cellular metabolism or exogenous agents such as irradiation or UV light.[55] Depending on damage type, base excision repair (BER) corrects alterations of DNA bases or nucleotide excision repair (NER) replaces oligonucleotides containing damaged bases. Also, mismatch repair (MMR) directly corrects mispaired DNA bases.[56-58] Poly-ADP ribose polymerase 1 (PARP1) is a well-known DNA damage sensing protein, especially in BER. In humans, the PARP family is comprised of 17 members, PARP1 being the major protein (> 90% of cellular PARP activities[59]) among of them. Once PARP1 recognizes DNA damage, it generates poly-ADP-ribose polymer chains (PARylation or PAR) on itself and other proteins. This posttranslational modification triggers further DNA damage response and recruits other repair molecules to the damage sites.[55]

10

Unlike SSBs, DSBs are considered the most deleterious type of DNA damage. This is because the damage in both strands of double helix causes a massive loss of genetic information, genome rearrangements, and cell death. To prevent these consequences, cells have developed two major repair pathways: HR and NHEJ.[56,60] HR utilizes a sister chromatid as a template to repair the break. As it faithfully restores the lost genetic information from the intact template, HR repair is considered an error-free repair method. Due to the availability of the sister chromatid, HR repair operates only during late S and G2 phase of the cell cycle.[61,62] DNA end-resection by CtIP is necessary for initiating HR repair. In this process, the pre-synaptic Rad51 filament is formed which is a long single-strand DNA coated with Rad51 recombinase, and it begins to search for its homologue. Other repair proteins such as RPA, BRCA1, and BRCA2 are also involved in this process.[60] On the other hand, NHEJ, the other major DSB repair, is active in all the phases of the cell cycle. NHEJ resolves DSBs fast because it simply catalyzes the rejoining reaction between two DNA ends. Therefore, NHEJ promotes a potentially inaccurate repair and is called error-prone repair. NHEJ starts with the binding of the ku70/80 heterodimer to both ends of the break, followed by the recruitment of other repair proteins such as DNA-dependent protein kinase (DNA-PKcs).[63,64]

In the nucleus, DNA is organized in the form of chromatin which consists of DNA, proteins (mainly histone) and RNA. It is widely accepted that chromatin near the DSBs should be relaxed to have a nucleosome-free DNA microenvironment which allows repair proteins to be recruited to the damage sites.[65-67] Therefore, change in chromatin configuration is necessary for efficient repair during DNA damage response. In fact, a large

number of chromatin modifying enzymes such as ATP-dependent chromatin remodelers and histone modifiers are known to be recruited to the DSB sites. Specifically, several studies have shown that INO80 [68-70] and NuA4/Tip60 [71-73] are recruited to the damaged chromatin in a γH2AX–dependent manner. These results suggest the importance of chromatin regulation during DNA repair, but how they regulate chromatin structure is not well understood.

At the same time, several researchers have provided valuable insights into the functional importance of SWI/SNF chromatin remodeling complex in DSB repair. BRG1, the SWI/SNF ATPase, promotes DNA damage repair by facilitating recruitment of XPC to regulate the UV-induced G1/S checkpoint, thus inactivation of BRG1 leads to increased UV-induced apoptosis.[74-76] Furthermore, inactivation of SNF5 causes UV hypersensitivity and inefficient CPD repair.[74,77]

Recently, emerging data propose that ARID1A also participates in DSB repair. Loss of ARID1A decreases NHEJ repair and increases sensitivity to damaging agents such as radiation, cisplatin, and UV. Also, inhibition of other subunits of SWI/SNF complex such as SNF5, BAF60a, BAF60c, BAF155, or BAF170 phenocopies the ARID1A loss.[78] The compromised NHEJ by loss of ARID1A may directly link to intrinsic platinum resistance observed in clear cell carcinomas. In mammals, the majority of DNA damaging lesions in normal cells are repaired by NHEJ pathway. Therefore, difference in functional dependency between normal cells and cancer cells on NHEJ repair pathway represents a therapeutic promise for cancer with DNA repair deficiency.

1-4. Exploitation of ARID1A Mutation as Therapeutic Target

As more evidence is showing that ARID1A mutation is prevalent in different types of cancers, researchers try to find an effective treatment to target ARID1A mutated cancers. Especially for genes with loss of function mutation, there is no way to target those mutated proteins. Therefore, the targeted therapy should not exploit the mutated proteins, but rather alterations in the biological pathways where these genes are involved. Two years ago, one group proposed that pharmacological inhibition of EZH2 methyltransferase sensitizes ARID1A mutated ovarian cancer.[79] Using a drug screening technique, they found that an EZH2 methyltransferase inhibitor, GSK-126, target highly specifically ARID1A mutated cancer by inhibiting the PI3K–AKT signaling pathway. However, EZH2 methyltransferase has not been used in clinics, so it requires a long period of time for developing safe inhibitors and validation. Another group presented a PARP inhibitor, BMN-673, as a promising drug to target ARID1A mutated cancer.[80] Though PARP inhibitor is currently used in clinic and known as a safe drug, drug resistance ultimately arises in many cases. However, this report had a significant impact because it showed a possibility of targeting DNA repair pathway as a promising drug for ARID1A mutated cancer.

Understanding DNA repair is critical in cancer treatment. Defects in DNA repair accumulate incorrect information and this leads to cancer predisposition. Most cancers present chromosomal instability (CIN), microsatellite instability (MIN) and accumulation of DNA base mutations and it is well known that cancer is an evolutionary disease encouraged by genomic instability.[81] In fact, genes encoding different components of the DNA damage response and DNA repair network are among the most commonly mutated

genes in cancer.[82-84] Though genomic instability in cancer provides several advantages by promoting dysregulated growth, tumor cell invasion and metastasis,[85-87] it makes the cells vulnerable to the DNA damaging agents and pharmacological inhibition of the DNA repair enzymes. Exploiting these lesions for targeted cancer therapy holds great promise but requires a fundamental understanding of the DNA repair collaterals.

DNA repair mechanisms greatly affect the response to cytotoxic treatments such as radiation and platinum-based chemo drugs. Especially for ionizing radiation (IR), this treatment induces a plethora of DNA lesions, including oxidative base damages and SSB, but mainly DSB which is the most lethal type of damage.[60] Though HR and NHEJ are able to repair radiation induced DSBs, NHEJ is thought to perform a major role in DNA repair throughout the entire cell cycle, while HR is limited to S and G2 phase.[88] Indeed, it is well established that cells with NHEJ defects, including mutations in DNA-PK or Ku70, are much more sensitive to radiation compared to normal cells.[89-92] Further efforts found that inhibition repair proteins involved in either HR, NHEJ or other DNA repair, such as BRCA1/2, ATM, ATR, CHK1, and PARP, also increases radiosensitivity.[93-97] Therefore, we need to utilize our understanding of cancer genetic signatures to radiation treatment, and maximize tumor cell killing and minimize the normal tissue side effects at the same time.

Recently, the concept of synthetic lethality has been successfully studied to target non-druggable cancer-specific genomic alterations. By definition, synthetic lethality happens when deficiencies in the two genes lead to cell death, whereas a deficiency in only one of these genes does not.[98,99] The most well-known example is PARP inhibitors in HR

14

deficient tumors, specifically BRCA1 or BRCA2 deficient breast and ovarian cancer.[100-102] PARP is well known to be involved mainly in BER, but accumulating evidence suggests that it is also associated with DSB repair.[103] There are two major mechanisms explaining how PARP inhibitors work in cancer treatment (**Figure 1-2**). The first one is that PARP inhibitors repress the SSB pathway and this converts SSBs into DSBs during S phase. As cells with HR defects fail to repair DSBs, BRCA deficient cells become sensitive to the PARP inhibitor.[104,105] The other mechanism is PARP trapping. The PARP inhibitor traps PARP on the DNA damage sites because the inhibitor catalytically inhibits interactions with NAD+ (nicotinamide adenine dinucleotide) which is required for PARP dissociation from the DNA damage site.[103,106,107] This trapped PARP-DNA complex will cause a replication fork collapse during S phase when HR is highly required. For this reason, it is possible that BRCA deficient cells are more sensitive to PARP inhibitors than BRCA proficient cells.[103] The important point of synthetic lethality is that it sensitizes only cancer cells who have DNA repair defects because normal cells can repair DSBs by either HR or NHEJ. By using this concept, we can increase target specificity with minimized side effect.

Hence, in this thesis project, we attempt to exploit an ARID1A mutation-based synthetic lethality screen. Based on our understanding of the function of ARID1A in DNA repair, we tried to find a molecule that causes synergistic cytotoxicity in ARID1A deficient cells. The first part of this thesis will discuss molecular function of ARID1A during DNA DSB repair. The second part will be about how to target ARID1A mutated cancer by using synthetic lethality. We hope that this endeavor leads to the identification of a highly effective therapy for cancer patients with ARID1A mutation.
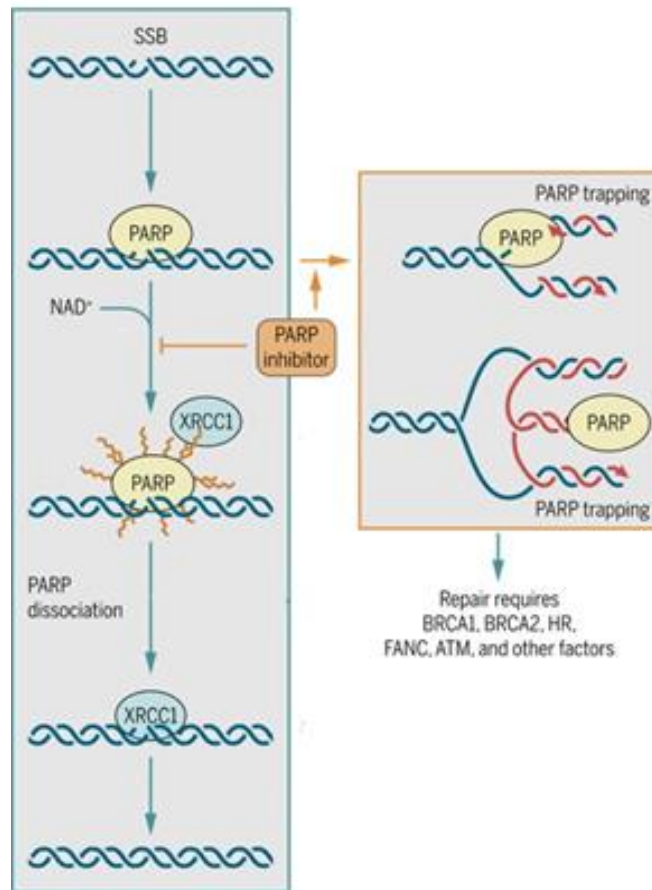
Figure 1-2. DNA repair by PARP and the effects of PARP inhibitors. (modified from reference [103]) Upon the generation of an SSB, PARP binds to the break and uses NAD+ to generate PAR polymers on itself (auto-PARylation) and other proteins which further recruits more repair proteins. PARP inhibitors bind to the NAD+ site of PARP and prevent PARP dissociation from the SSB, resulting in both accumulations of unrepaired SSBs and PARP trapping. In order to repair the ensuing DSBs caused by PARP trapping during DNA replication, cells require BRCA1, BRCA2, and other HR factors.

Chapter 2: The Caretaker Role of ARID1A

in DNA DSB repair

2-1. ARID1A deficiency is associated with sustained DDR and DSBs *in vivo*

To study the role of ARID1A in the DNA damage response (DDR), we first quantified DSBs in human endometrial tissue containing Endometrial Intraepithelial Neoplasm (EIN or CAH; Complex Atypical Hyperplasia, the precursor lesion to endometrioid carcinoma), which often exhibits focal loss of ARID1A (**Figure 2-1**). Immunohistochemical staining for phosphorylated H2AX (S139, γH2AX), a marker of DSBs, revealed higher intensity staining in ARID1A negative areas, compared to cells with intact ARID1A expression. Since we have previously observed increased proliferation upon depletion of ARID1A, in order to confirm that increased γH2AX staining was truly reflective of DSBs rather than proliferation, we also stained tissues with phosphorylated ATM (S1981, pATM). A key mediator of the DDR, ATM undergoes autophosphorylation at S1981 in response to DSBs, independent of proliferation status. We observed concordance in pATM staining with γH2AX, implying that unrepaired DSBs are more prevalent in ARID1A deficient cells.

To functionally establish the role of ARID1A in DSB repair, we employed a conditionally inducible ARID1A knock-out mouse model (**Figure 2-2**), generated by crossing ARID1A^flox/flox mice with mice carrying doxycycline-inducible Cre recombinase under control of the Pax8 promoter to drive tissue-specific expression. Pax8 is a transcription factor expressed in epithelial cells lining the gynecologic tract, including endometrial epithelial cells (but not stromal cells) and fallopian tube secretory cells; thus, in our mouse model, doxycycline administration causes Pax8-driven inactivation of ARID1A in Mullerian epithelium.

Treatment of mice for 1 week with doxycycline resulted in a mosaic pattern of ARID1A expression in endometrium, mimicking the heterogeneous loss of ARID1A in human CAH, while enabling the evaluation of markers of DNA damage (γH2AX) and DDR (phosphorylated Kap1 (S824, pKAP1)) in ARID1A-knockout (ARID1A-KO) cells compared to cells retaining its expression. We resorted to measuring pKap1, a downstream substrate of ATM[108] due to the inavailability of effective commercial pATM antibodies for mouse tissue. Whole-animal irradiation was performed to generate DSBs. Immunohistochemical staining revealed more prominent γH2AX punctuate foci in ARID1A-KO cells at 2 h and 8 h post-irradiation (7- and 3-fold increase, respectively) compared to ARID1A intact cells. Differences in pKAP1 nuclear staining were observed as early as 5 min after radiation exposure, with enhanced immunoreactivity in ARID1A-KO cells. Taken together, these results are consistent with involvement of ARID1A in DSB repair and that its loss leads to a delayed DDR.
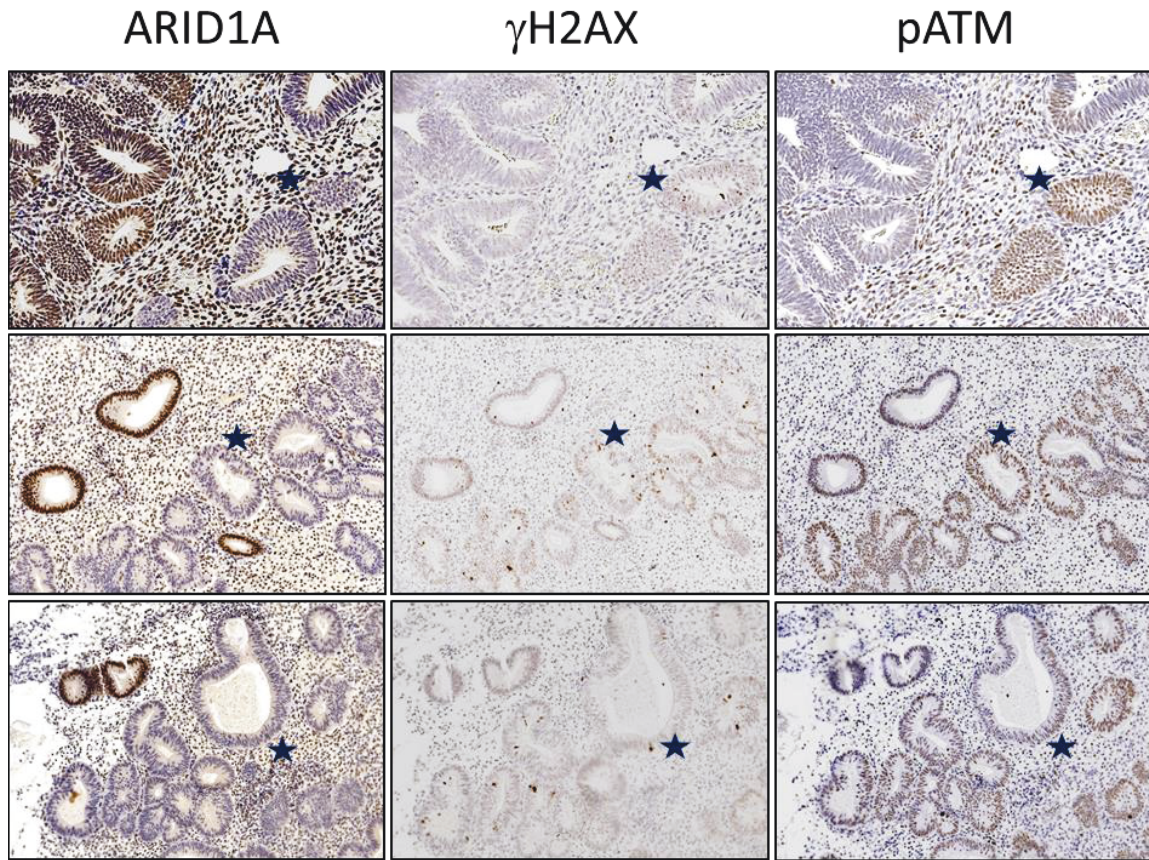
Figure 2-1. The level of DDR and DSBs in human EIN tissues. The representative images of immunohistochemistry with ARID1A, γH2AX and phosphorylated-ATM (s1981) in human Endometrial Intraepithelial Neoplasm (EIN) tissue were shown. ARID1A deficient areas were marked with blue stars.

A

Doxycycline (Oral gavage) → *Arid1a* knock-out (Müllerian lineage specific promoter) → Irradiation (2.5Gy) → Isolate uterus after 2h or 8h

B

	ARID1A	γH2AX	pKAP1
NO IR			
2h			
8h			

C

γH2AX foci / cell

***

**
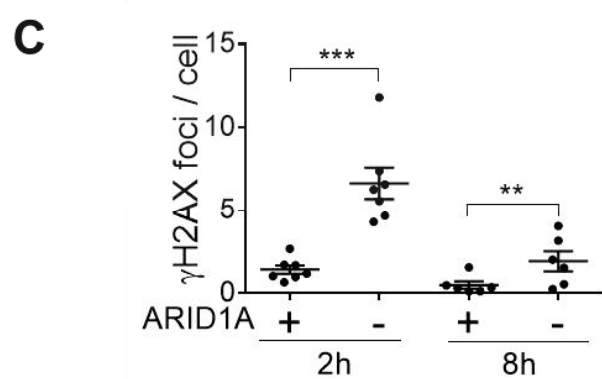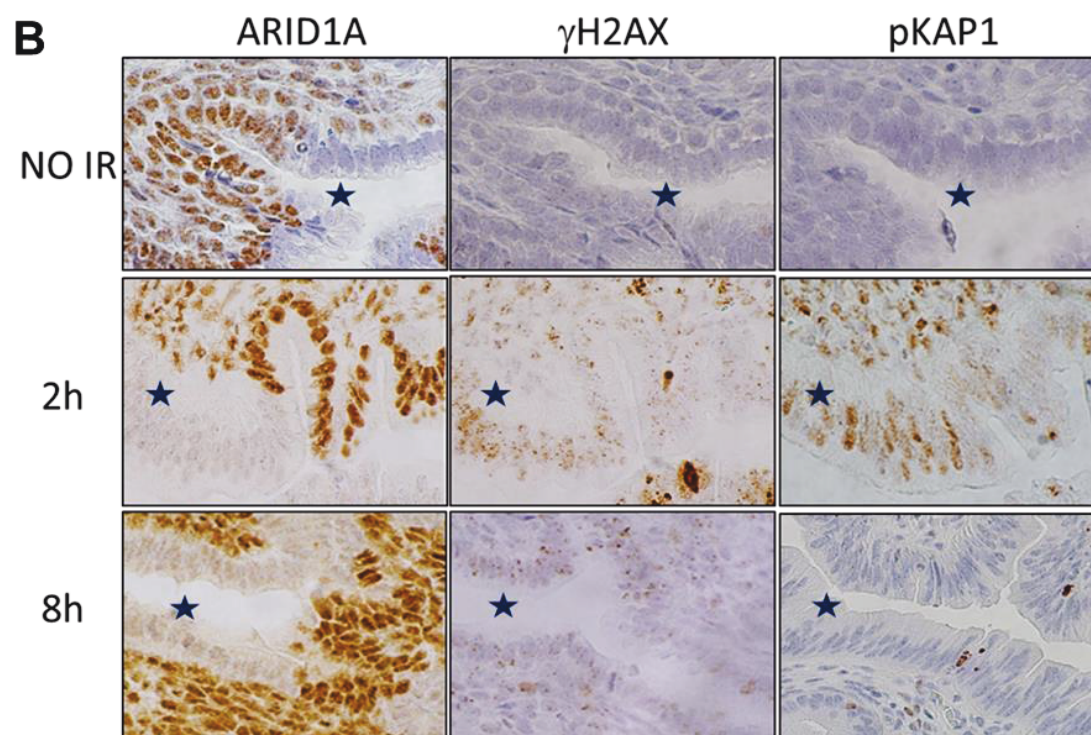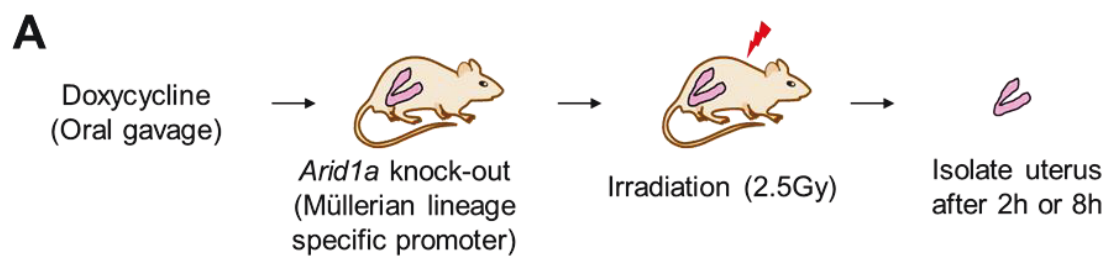
ARID1A + − + −
        2h   8h

Figure 2-2. The change of γH2AX level after irradiation in mouse endometrial tissues.

(A) Schematic representation of mouse irradiation experiment was shown. (B) The representative images of immunohistochemistry with ARID1A, γH2AX and phosphorylated-KAP1 in mouse uterus tissue were shown. Mice were treated with doxycycline for one week and sacrificed at the indicated time points after irradiation (2.5Gy). ARID1A deficient areas were marked with blue starts. (C) Quantitation of γH2AX foci per each endometrial epithelial cell was shown. Data was represented as a mean ± SEM, n>500. n>15. * $p < 0.05$, ** $p < 0.01$, *** $p < 0.001$

2-2. ARID1A deficiency compromises DNA DSB repair

To further characterize its role in DSB repair, ARID1A was deleted in an immortalized endometrial epithelial cell line, hEM3, by CRISPR (**Figure 2-3**). Consistent with our *in vivo* observations, γ-irradiation resulted in higher levels of γH2AX in hEM3-ARID1A$^{-/-}$ cells relative to control hEM3-ARID1A$^{+/+}$ cells at all time-points; in particular, by 8h post-irradiation, ARID1A$^{+/+}$ cells have completely repaired DSBs, as evidenced by return of γH2AX to basal levels, while it was still elevated 3-fold over baseline in ARID1A$^{-/-}$ cells. These results were verified by silencing ARID1A in the parental hEM3 cell line by two non-overlapping siRNAs, excluding the possibility of single-cell clone-derived effects. Similar findings were also obtained from ARID1A isogenic MCF10A cells (**Figure 2-3**).

Next, we investigated whether enforced ARID1A expression in an ARID1A deficient background is able to promote DSB repair (**Figure 2-4**). OVISE ovarian clear cell carcinoma cells and HEC1A endometrial carcinoma cells, which originally harbor ARID1A deletion mutations, were engineered to carry a doxycycline-inducible ARID1A construct. In both cell lines, induction of ARID1A expression after 48h doxycycline treatment resulted in diminished γH2AX under basal conditions and at all the time points after irradiation.

Immunofluorescence was performed to visualize and quantify γH2AX foci after irradiation (**Figure 2-5**). Again, we found that ARID1A-deficiency, through either knockout or knockdown, was associated with higher numbers of γH2AX foci relative to controls, while they were reduced with ARID1A re-expression. DNA damage was directly quantified by the neutral comet assay, using 'tail moment,' derived from multiplying tail

23

intensity by length, as a measure of the extent of DSBs (**Figure 2-6**). Irradiation resulted in higher tail moments in ARID1A deficient compared to ARID1A intact cells, with phenotypic rescue achieved by ARID1A re-expression. Together, these results suggest that ARID1A participates in DSB repair and that its loss results in the persistence of DNA fragmentation after irradiation.

Given the deleterious effects of DNA damage, the impact of ARID1A on cell survival after irradiation was evaluated (**Figure 2-7**). Cells were exposed to increasing doses of radiation, and cell viability was measured by Cell-Titer Blue at 72h post-treatment. Compared to ARID1A deficient cells, ARID1A intact cells exhibited increased resistance to irradiation. Differences in survival between ARID1A intact and ARID1A deficient cells became apparent at 2 Gy and increased in a dose-dependent manner. The effects were most pronounced in MCF10A cells at 5 Gy (20% survival in ARID1A$^{-/-}$ compared to >60% in ARID1A$^{+/+}$ cells). Next, colony forming ability was assessed by crystal violet staining on Day 5 post-irradiation (**Figure 2-7**). In accordance with short-term viability assays, ARID1A deficient cells exhibited decreased colony formation compared to controls, implicating a protective role of ARID1A in response to DNA damage. Collectively, these results support a caretaker role of ARID1A in mammalian cells in the regulation of the DNA damage response.
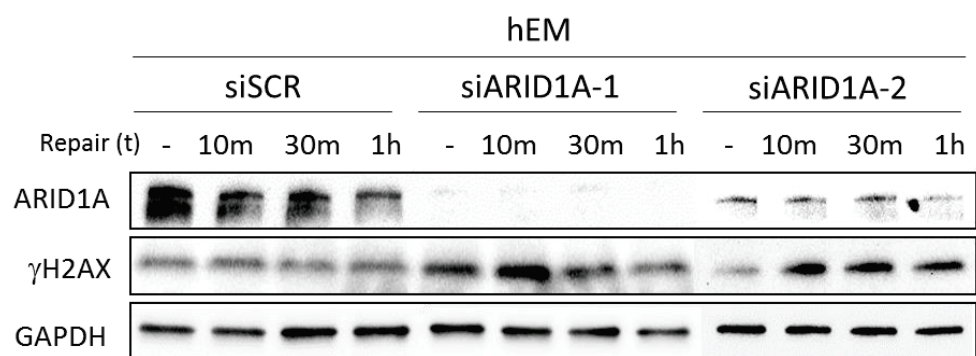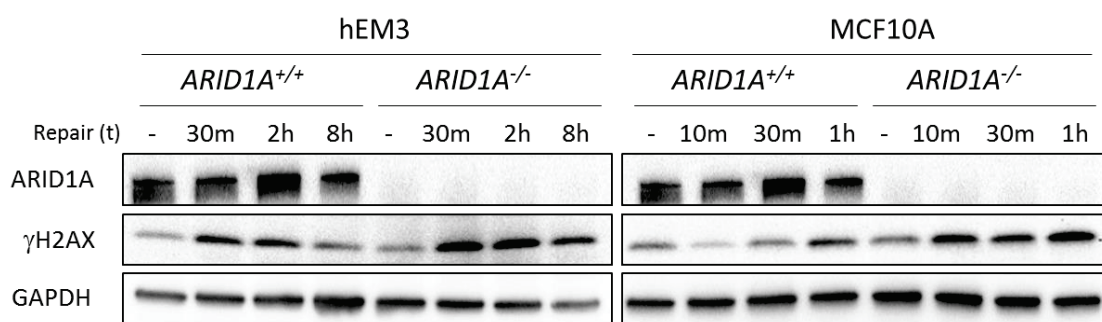
Figure 2-3. The change of γH2AX level after irradiation in cells. Immunoblotting analysis showed levels of ARID1A and γH2AX in hEM3 and MCF10A cells. GAPDH was used as a loading control. Cells were analyzed at the indicated time points after irradiations.
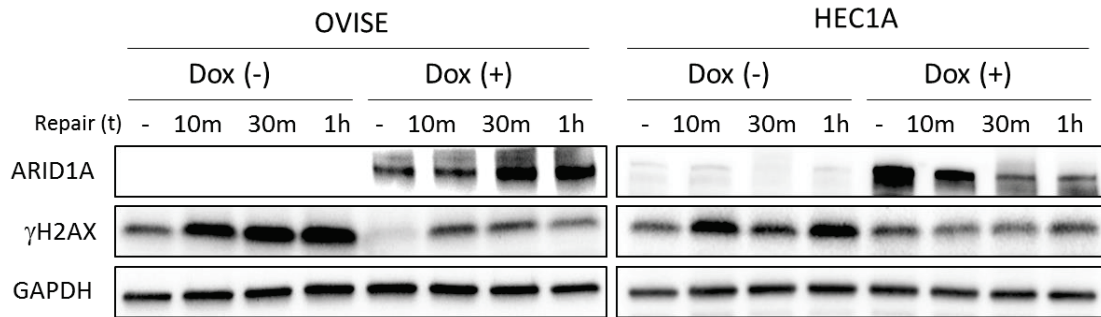
Figure 2-4. γH2AX in ARID1A mutated cancers with or without ARID1A re-expression. Immunoblotting analysis showed levels of ARID1A and γH2AX OVISE and HEC1A cells. In Dox (+) group, cells were treated with 1ug/ml doxycycline for 2 days. On the other hand, cells were treated vehicle in Dox (-) group. GAPDH was used as a loading control. Cells were analyzed at the indicated time points after irradiations.
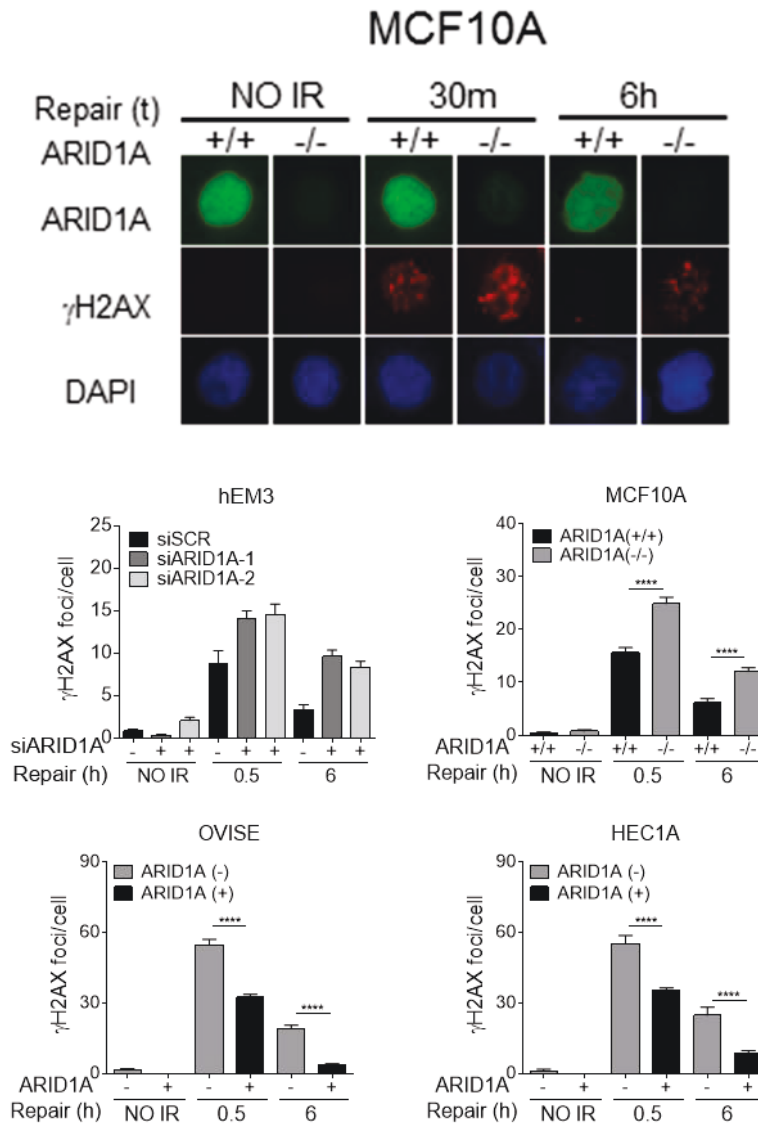
Figure 2-5. Quantification of γH2AX foci after irradiation by immuncytostaining. The representative images of immunocytochemistry with ARID1A, γH2AX and DAPI in MCF10A cells were shown. MCF10A, hEM3 cells transfected with siRNAs, ARID1A inducible OVISE and HEC1A cells were analyzed at the indicated time points after irradiation (4Gy). Quantitation of γH2AX foci per cell was shown. Data was presented as a mean ± SEM, n>15. * p<0.05, ** p<0.01, *** p<0.001
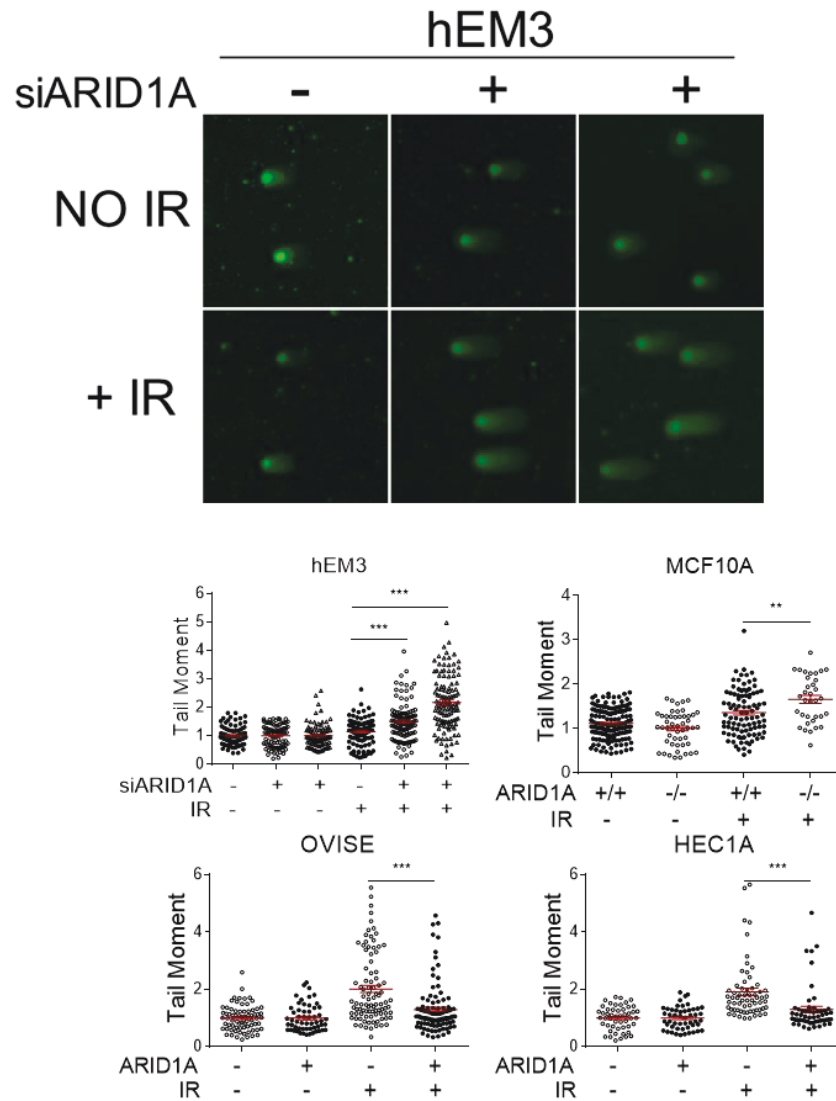
Figure 2-6. Quantification of DSBs by neutral comet assay. The representative images and quantification of neutral cell comet assay in hEM3 cells were shown. MCF10A, hEM3 cells transfected with siRNAs, ARID1A inducible OVISE and HEC1A cells were analyzed 30min after irradiation (4Gy). Tail moment was calculated by multiplying the tail intensity and length. Data was presented as a mean $\pm$ SEM, n>50. * $p<0.05$, ** $p<0.01$, *** $p<0.001$
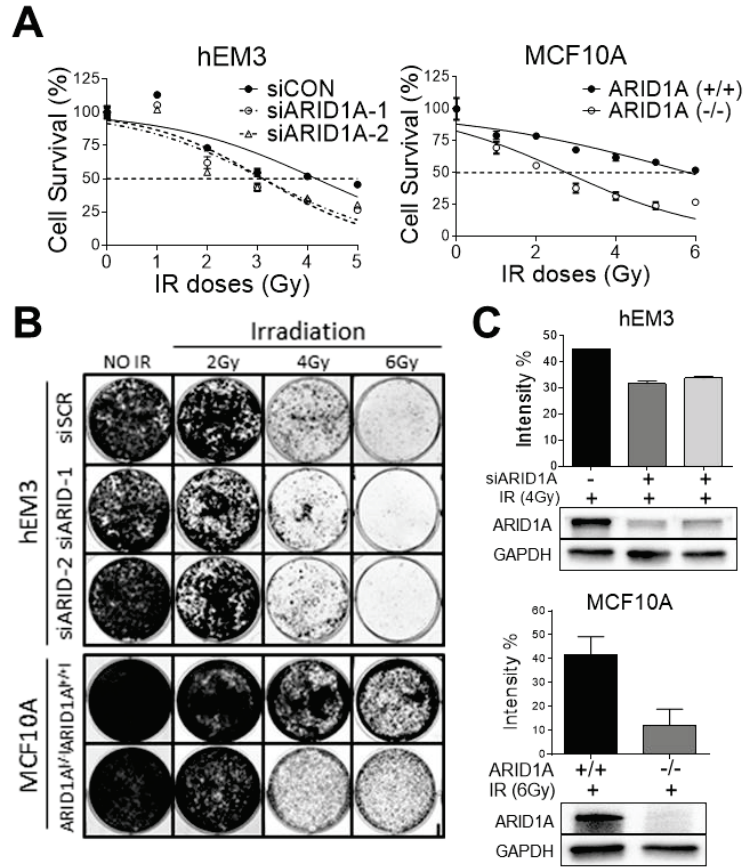
Figure 2-7. Cell cytotoxicity after irradiation. (A) Cell survive curves for hEM3 cells transfected with siRNAs and MCF10A cells were presented. 1×10^3 of cells wew seeded for 24 hours and differentially irradiated. Cell viability was measured by cell titer blue on day 4. Data was presented as a mean ± SEM of triplicates. (B-C) Representative images and quantitative analysis of the colony forming assay were presented in hEM3 cells transfected indicated siRNAs and MCF10A cells. 1×10^4 of indicated cells were seeded for 24 hours and differentially irradiated as indicated. Colonies were visualized with crystal violet on day 5. Immunoblotting analysis showed ARID1A level and GAPDH was used as a loading control. Data was presented as a mean ± SEM of two individual experiments. * p<0.05, ** p<0.01, *** p<0.001

2-3. The recruitment of ARID1A to DNA DSBs is critical for the mobilization of histones.

Since SWI/SNF complexes function as master regulators of chromatin structure, we hypothesized that the ARID1A-chromatin interaction is a key component of the cellular response to DSBs. First, to determine whether ARID1A is recruited to DSBs, 405nm laser-induced microirradiation was used to generate DNA damage localized to a single horizontal line across the nucleus (verified by γH2AX immunostaining) in cells transfected with GFP-tagged ARID1A (**Figure 2-8**). Live-cell imaging, performed to monitor the localization of ARID1A over time, revealed rapid recruitment of ARID1A to DSBs, represented by enhanced GFP signal at the site of micro-irradiation.

The SWI/SNF complexes remodel chromatin by mobilizing nucleosomes in an ATP-dependent manner. Normally, the H2B core histones are tightly bound to DNA and together with other histone proteins, form the structural core of the nucleosome. To visualize the ejection of nucleosomes from chromatin, histone H2B tagged with PAGFP, a photoactivatable version of GFP, was transfected into ARID1A intact and deficient cells (**Figure 2-9**). Localized DSBs and photoactivation of H2B-PAGFP were induced by laser micro-irradiation. As only H2B-PAGFP proteins at the site of DNA damage were activated by the laser, any GFP signal detected outside this area represents H2B-PAGFP proteins evicted from the original site of DSB. Comparison of histone mobility between ARID1A$^{+/+}$ and ARID1A$^{-/-}$ cells by measuring fluorescent signal at non-damaged areas (yellow box) revealed increased fluorescence over time in both groups, but the magnitude of the change

was much higher in ARID1A$^{-/-}$ cells, supporting a role of ARID1A in the eviction of histones.

Next, we monitored fluorescence recovery after photobleaching (FRAP) after laser-induced microirradiation of cells expressing histone H2B-GFP (**Figure 2-9**). The recovery of GFP represents the incorporation of free histone H2B-GFP into DSB sites. In this experiment, we found that the GFP signal at the DSB sites recovered more quickly in cells with ARID1A than in cells without ARID1A. Collectively, the data demonstrate that ARID1A is recruited to the site of DNA DSB to promote the mobilization of histones.

Furthermore, we wanted to confirm if the difference of histone dynamics only occurs during DSB repair, we applied microirraidaition with reduced laser intensity which is enough to cause photobleaching but DSBs (**Figure 2-10**). In this condition, we could not observe any noticeable difference of histone dynamics between ARID1A wildtype and deficient cells. Therefore, we concluded that ARID1A facilitates histone mobility corresponding to DSB repair.
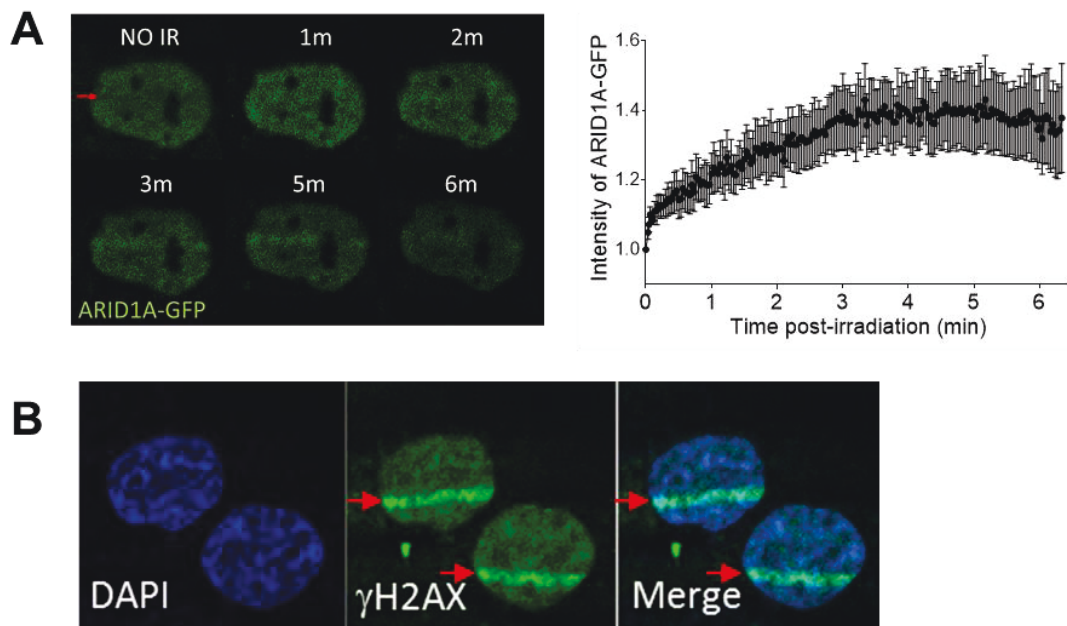
Figure 2-8. Localization of ARID1A at the DSB sites and its kinetics. (A) The representative live images of hEM cells transfected with ARID1A-GFP (Green) plasmids at the indicated time points after microirradiation (red arrow). The GFP intensity at the DSB sites was plotted after normalization by background and its basal intensity. Data was presented as a mean ± SEM, n>10 (B) The representative images of immunocytochemistry with DAPI (blue), γH2AX (green) and Merge in hEM cells were shown. A region of the nucleus (red arrow) was microirradiated with 405nm laser (100% power output with 4 laser iterations) after 10 minutes incubation with Hoechst (2ug/ml).
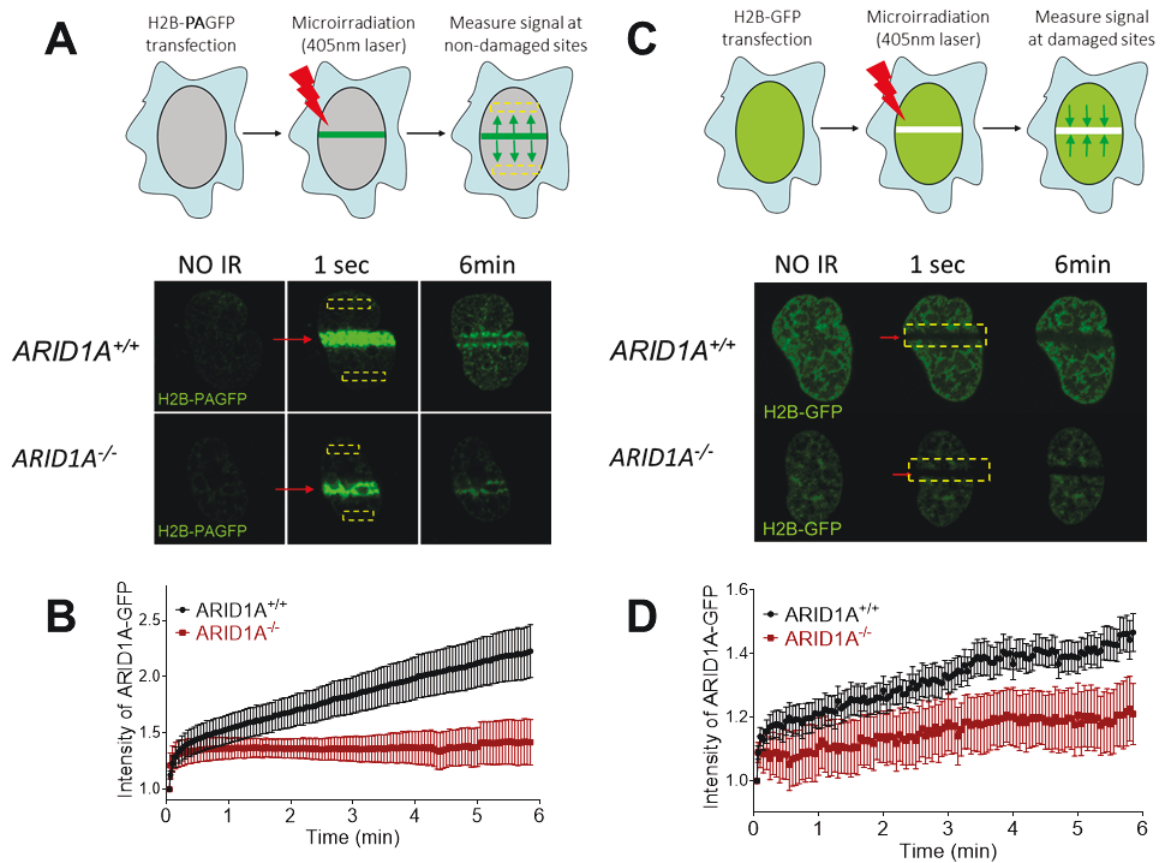
Figure 2-9. Kinetics of histone dynamics at the DSB sites. (A) Schematic representation and representative live images of hEM cells transfected with H2B-PAGFP were shown at the indicated time points after microirradiation (red arrow). (B) Intensity of GFP in non-irradiated area (yellow box) was measured every 3 seconds before and after micoirradiation until 6 minutes. The GFP intensity was plotted after normalization by background and its basal intensity. Data was presented as a mean ± SEM, n>11 (C) Schematic representation and representative live images of hEM cells transfected with H2B-GFP were shown at the indicated time points after microirradiation (red arrow). (D) Intensity of GFP in irradiated area (yellow box) was measured every 3 seconds before and after micoirradiation until 6

minutes. The GFP intensity was plotted after normalization by background and its basal

intensity. Data was presented as a mean ± SEM, n>17
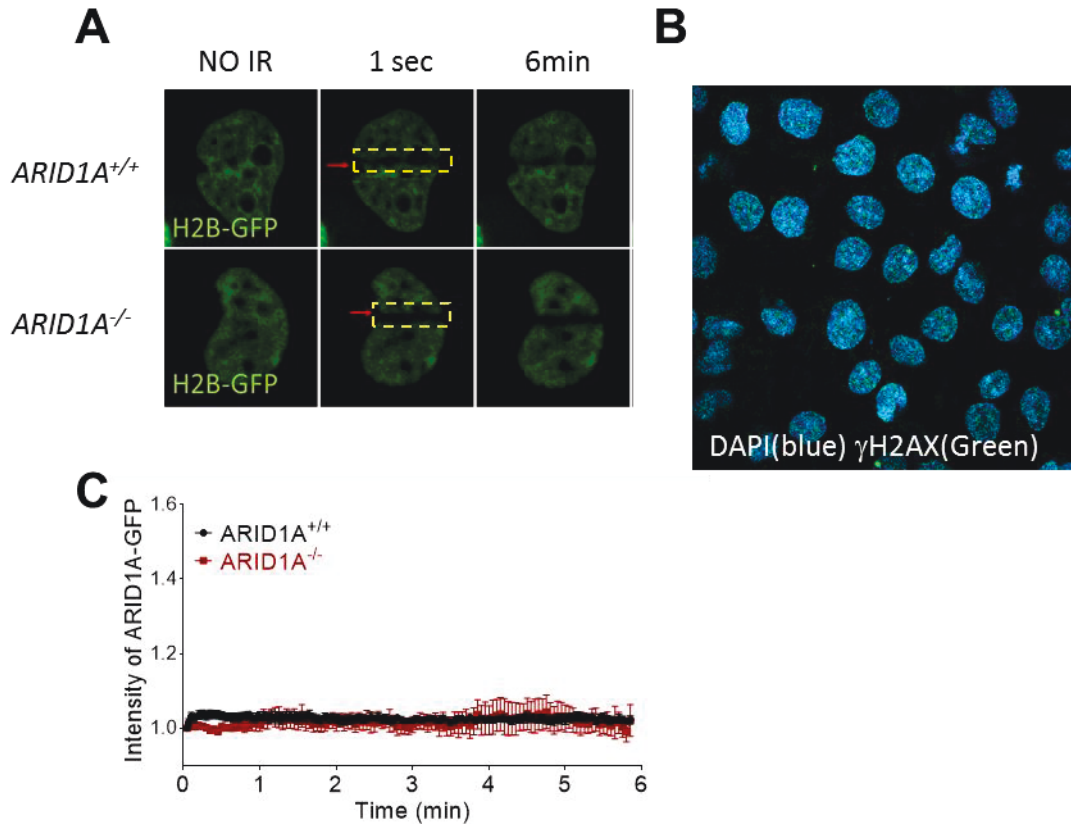
Figure 2-10. Kinetics of histone dynamics at the non-DSB sites. (A) Representative live images of hEM cells transfected with H2B-GFP were shown at the indicated time points after reduced microirradiation (405nm laser with 40% power output with 2 laser iterations). (B) The representative images of immunocytochemistry were shown with DAPI (blue), γH2AX (green) and Merge after microirradiated with reduced laser. (C) Intensity of GFP in irradiated area (yellow box) was measured every 3 seconds before and after micoirradiation until 6 minutes. The GFP intensity was plotted after normalization by background and its basal intensity. Data was presented as a mean ± SEM, n>6

2-4. ARID1A is essential for chromatin decondensation and accessibility at the DSB site.

To evaluate the impact of ARID1A loss on chromatin dynamics at the damaged sites, H2B-GFP-transfected cells were exposed to laser-induced microirradiation to induce DSBs while simultaneously photobleaching H2B-GFP; as this effectively 'labels' histone-associated chromatin, the size of the non-fluorescent region serves as a surrogate measure of chromatin compaction (**Figure 2-11**). At 2 min, this area increased significantly in ARID1A$^{+/+}$ cells, but only minimal deviation from baseline was observed in ARID1A$^{-/-}$ cells. To confirm that we were observing a specific response to DNA damage, cells were micro-irradiated with reduced laser intensity to cause photobleaching without generating DSBs; this did not result in any noticeable difference of chromatin relaxation between ARID1A intact versus deficient cells. Similar results were obtained using the H2B-PAGFP system, in which the increase in the fluorescent area at 2 min post-micro-irradiation was only observed in ARID1A$^{+/+}$ cells (**Figure 2-12**). Thus, the data suggest that ARID1A is involved in chromatin decondensation following DSB.

Since the decompaction of chromatin was inferred indirectly through measurements of H2B, further validation was performed using the Assay for Transposase-Accessible Chromatin sequencing (ATAC-seq) to directly assess chromatin accessibility genome-wide; the technique relies on hyperactive Tn5 transposase to simultaneously fragment DNA and ligate adaptors for sequencing relatively accessible regions of the genome. (**Figure 2-13**). We performed ATAC-seq on ARID1A intact and deficient cells before and after irradiation and quantified the distribution of fragment lengths. Since

radiation-induced DSBs cause random fragmentation of DNA, we focused our analysis on fragments around 146bp in length, corresponding to mono-nucleosomes. Enrichment of mono-nucleosomes is indicative of an open chromatin state. As to be expected, in ARID1A$^{+/+}$ cells, a higher mono-nucleosome peak was observed after irradiation, consistent with a global increase in chromatin accessibility in response to radiation. In contrast, the fragment length profiles before and after irradiation were similar in ARID1A$^{-/-}$ cells. This lack of enrichment for mononucleosomes in ARID1A$^{-/-}$ cells post-irradiation, implies that ARID1A plays a functional role in modulating chromatin state in response to radiation-induced DNA damage.

To interrogate chromatin accessibility specifically near DSBs, we introduced a site-specific DSB by CRISPR/Cas9 in ARID1A$^{+/+}$ and ARID1A$^{-/-}$ cells (**Figure 2-14)**. Extracted chromatin was subjected to an assay that relies on the differential sensitivity of open and closed chromatin to nuclease digestion. In brief, quantitative PCR was performed using specific primers placed near the site of DSB, on nuclease-digested and non-digested chromatin. The chromatin configuration could then be inferred from the differential abundance of amplifiable fragments, which, in turn, is dependent on the accessibility of the chromatin to nuclease. As expected, we observed increased chromatin accessibility within close proximity to the DSB (up to ~300bp) in ARID1A$^{+/+}$ cells compared to ARID1A$^{-/-}$ cells. No significant differences were observed near GAPDH, which is remotely located from the site of DSB. Therefore, ARID1A causes chromatin remodeling specifically within the vicinity of DSBs.
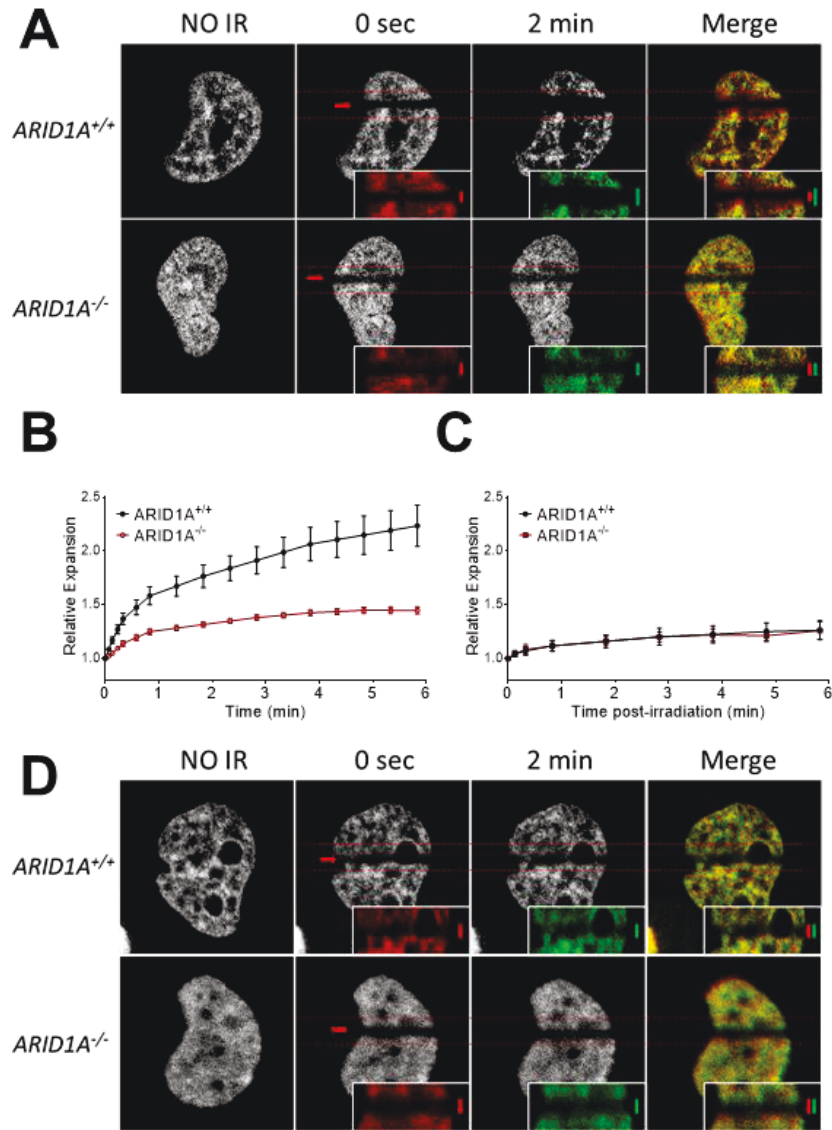
Figure 2-11. Quantification of damaged chromatin expansion by using H2B-GFP. (A) The representative live images of hEM cells transfected with ARIDIA-GFP. The damaged chromatin was marked with photobleaching with microirradiation. (B) The chromain expansion was plotted as a graph. Data was presented as a mean ± SEM, n>20 (C-D) Same as (A-B) but with reduced microirraidation. (40% with 2 literations)
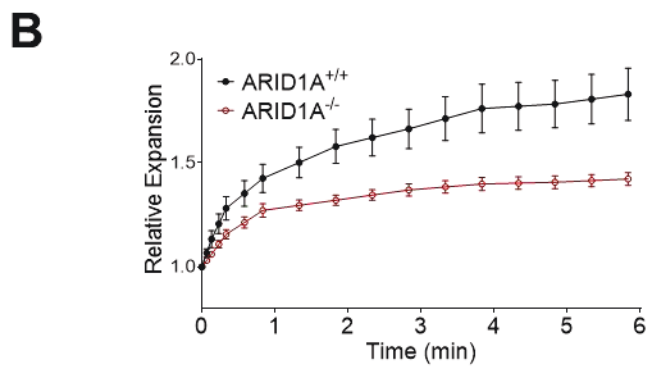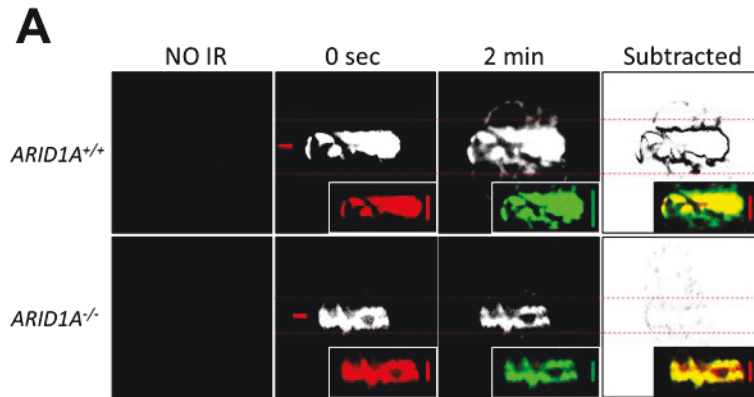
Figure 2-12. Quantification of damaged chromatin expansion by using H2B-PAGFP.

(A) The representative live images of hEM cells transfected with ARIDIA-PAGFP. The damaged chromatin was marked with photobleaching with microirradiation. (B) The chromain expansion was plotted as a graph. Data was presented as a mean ± SEM, n>10
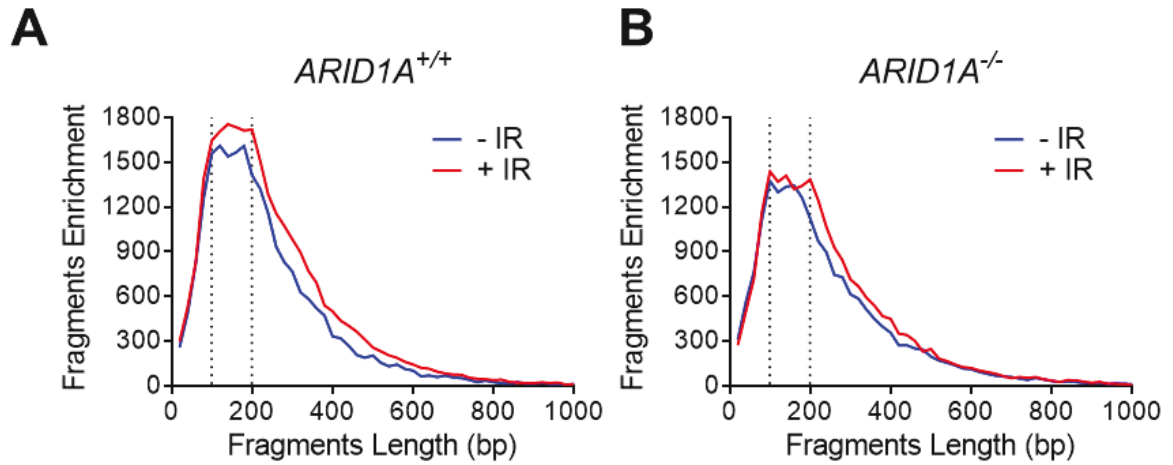
Figure 2-13. Global chromatin accessibility after irradiation through ATAC-sequencing. ATAC-sequencing was performed on ARID1A^{+/+} hEM cells (A) and ARID1A^{-/-} (B) hEM cells with (red line) or without irradiation (blue line) 1hour after 4Gy irradiation. 100 and 200 base pair of fragment length (near mono-nucleosome size) were marked with dash lines.
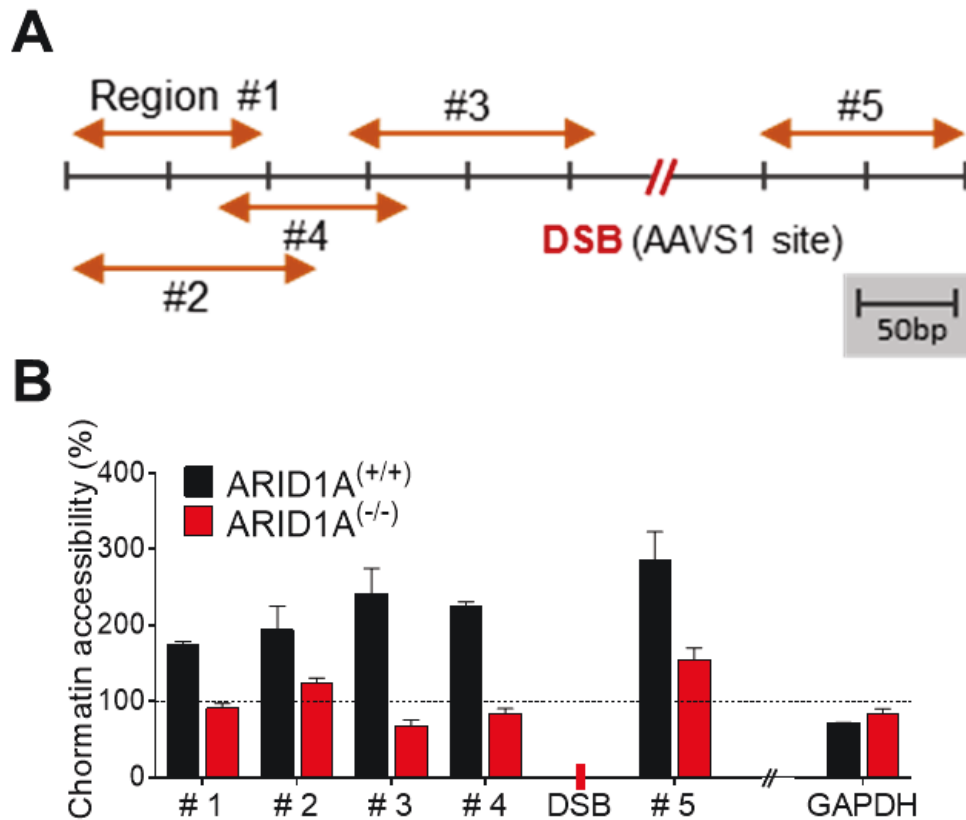
Figure 2-14. Local chromatin accessibility around DSB sites. (A) Schematic representation of DSB site (red color) and amplified areas (orange arrow) by specific primers on the genomic locus was presented. Eight hours after transfection with CRISPR/Cas9 containing plasmids (2ug), chromatin was isolated from hEM3 cells. (B) According to the manufacturer instruction, each region was amplified and chromatin accessibility was calculated. Each value was normalized by the chromatin accessibility on the basal condition (transfected with 2ug of vehicle plasmids). Data was presented as a mean ± SEM of two individual experiments.

2-5. ARID1A is necessary for the recruitment of NHEJ repair proteins to DSBs.

The traffic light reporter system was used to assess the impact of decreased chromatin accessibility, secondary to ARID1A deletion, on the functionality of NHEJ and HR (**Figure 2-15**). In brief, the reporter system, described in detail previous paper[109], consists of an embedded nuclease cleavage site, such that repair of nuclease-induced DSB generates distinct fluorescent signals depending on whether repair was mediated through HR (using an co-transfected donor template) or error-prone NHEJ. In the former situation, a functional GFP open reading frame is restored by the donor template, resulting in GFP+ cells, while in the latter case, a +2 frameshift (expected frequency of 1/3 of insertions/deletions) places an mCherry coding sequence in frame, resulting in mCherry+ cells. Quantification of GFP+ and mCherry+ cells following transfection of cleaved or intact construct into the isogenic cell line pair revealed a significantly lower fraction of mCherry+ cells induced by DSB in ARID1A$^{-/-}$ cells compared to ARID1A$^{+/+}$ cells. Since HR occurred in only a minor fraction of cells even in the presence of ARID1A, comparisons with ARID1A$^{-/-}$ cells were difficult to precisely quantify. Nevertheless, there was also an observable decrease in HR efficiency in the absence of ARID1A. Therefore, ARID1A loss causes a generalized impairment in DNA repair; however, the impact on NHEJ appears to be of greater biologic significance, since the vast majority cells rely on this pathway, at least in our model system.

To confirm that the ARID1A-dependent open chromatin state is necessary for interaction between repair proteins and damaged DNA, we monitored the recruitment of

53BP1, a key component of the NHEJ repair machinery, in ARID1A$^{+/+}$ and ARID1A$^{-/-}$ cells following laser micro-irradiation (**Figure 2-16**). We found that ARID1A deficiency significantly reduced 53BP1 recruitment to the DSB sites. Moreover, the reintroduction of ARID1A into ARID1A deficient cells partially restored 53BP1 recruitment, demonstrating a crucial role of ARID1A in mediating the physical interaction between 53BP1 to damaged DNA. The recruitment of RIF1, a crucial effector of NHEJ repair, located downstream of 53BP1, was also significantly impaired in ARID1A deficient cells (**Figure 2-17**).

To assess whether ARID1A recruitment to DSBs can, in turn, be affected by 53BP1, we evaluated ARID1A recruitment following siRNA-mediated knockdown of 53BP1 in hEM3 cells, and compared immortalized wildtype and 53BP1-knockout mouse embryonic fibroblast (MEF) cells (**Figure 2-18**). In both cases, we did not observe any noticeable difference in ARID1A recruitment between 53BP1 intact and deficient cells, indicating that there is no evidence for reciprocal regulation of ARID1A recruitment to DSBs by 53BP1. Collectively, our results demonstrate that the closed chromatin configuration secondary to ARID1A deficiency compromises NHEJ repair, by preventing the physical interaction of key repair proteins, including 53BP1 and RIF1, with DNA at the sites of DSB.
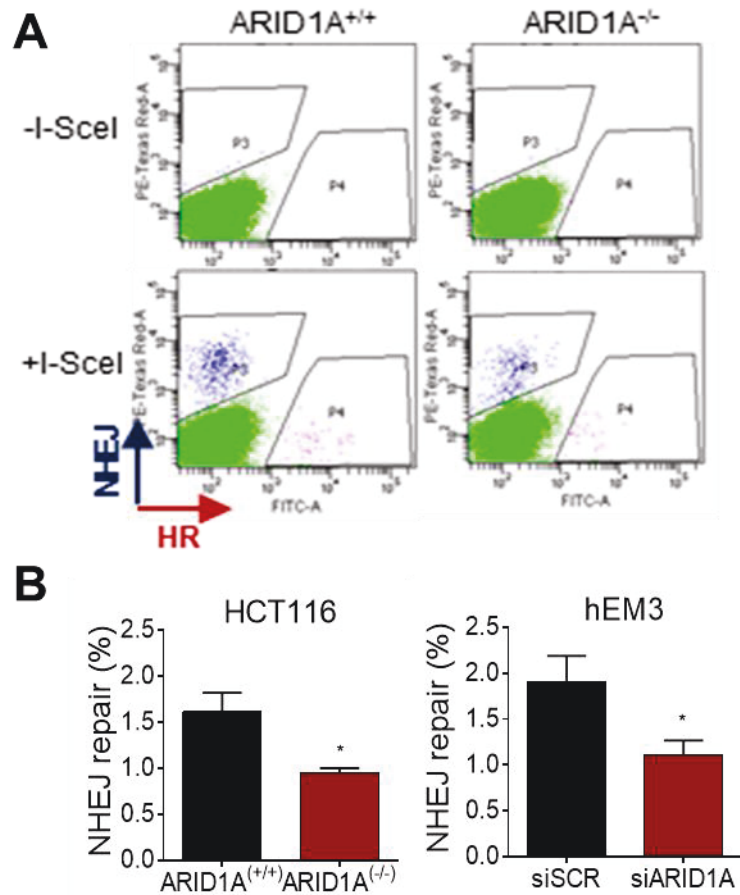
Figure 2-15. Quantification of NHEJ and HR by using TLR assay. (A) Flow cytometry analysis of hEM3^{TLR} and HCT116^{TLR} cells 72 h after transduction with the I-Sec/GFP donor lentiviral construct was performed. (B) The percentages of the NHEJ underwent cells (mCherry+, presented as blue dots in this figure) was presented as graphs. Data was presented as a mean $\pm$ SEM, n=3, * p<0.05, ** p<0.01, *** p<0.001
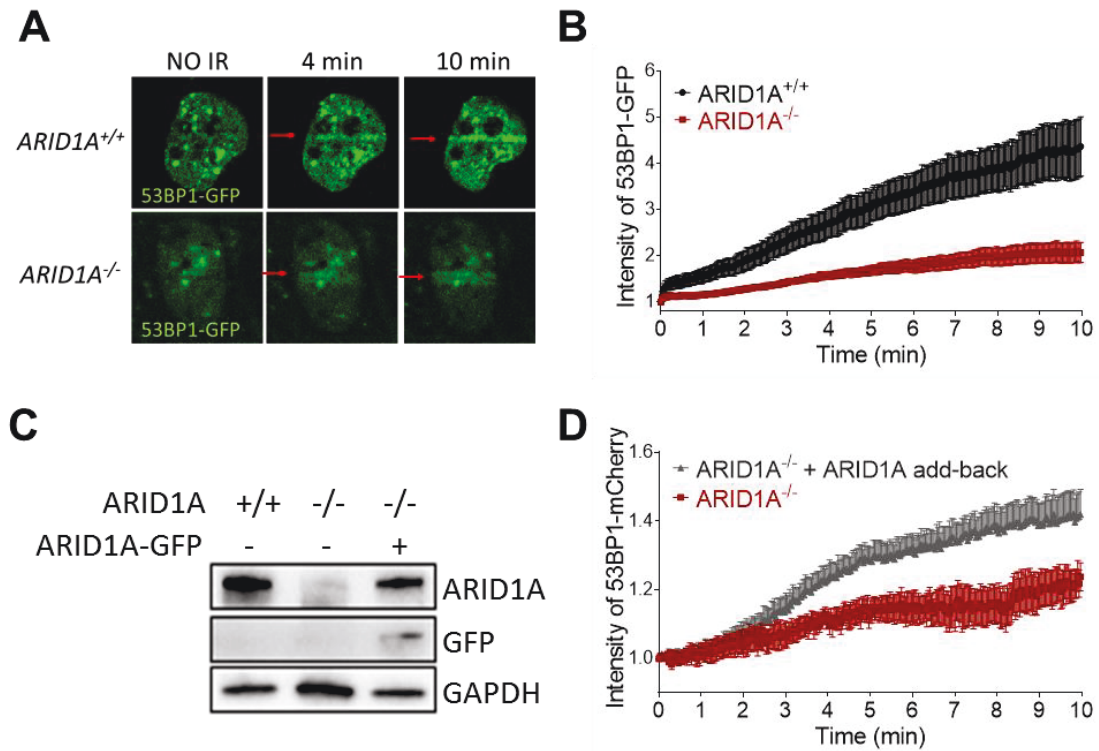
Figure 2-16. Quantification of 53BP1 recruitment at the DSB sties. (A) Representative live images of hEM cells transfected with 53BP1-GFP were shown at the indicated time points after microirradiation (red arrow). (B) Intensity of GFP at irradiated area (yellow box) was measured every 3 seconds before and after micoirradiation. The GFP intensity was plotted after normalization by its background and basal intensity. Data was presented as a mean ± SEM, n>7 (C) Immunoblotting analysis showed levels of ARID1A, GFP in hEM3 cells transfected with or without ARIDA-GFP plasmid. GAPDH was used as a loading control. (D) The mCherry intensity at irradiated area was measured every 3 seconds in ARID1A deficient hEM cells transfected with 53BP1-mCherry or 53BP1-mCherry and ARID1A-GFP. The mCherry intensity was plotted after normalization by its background and basal intensity. Data was presented as a mean ± SEM, n>6
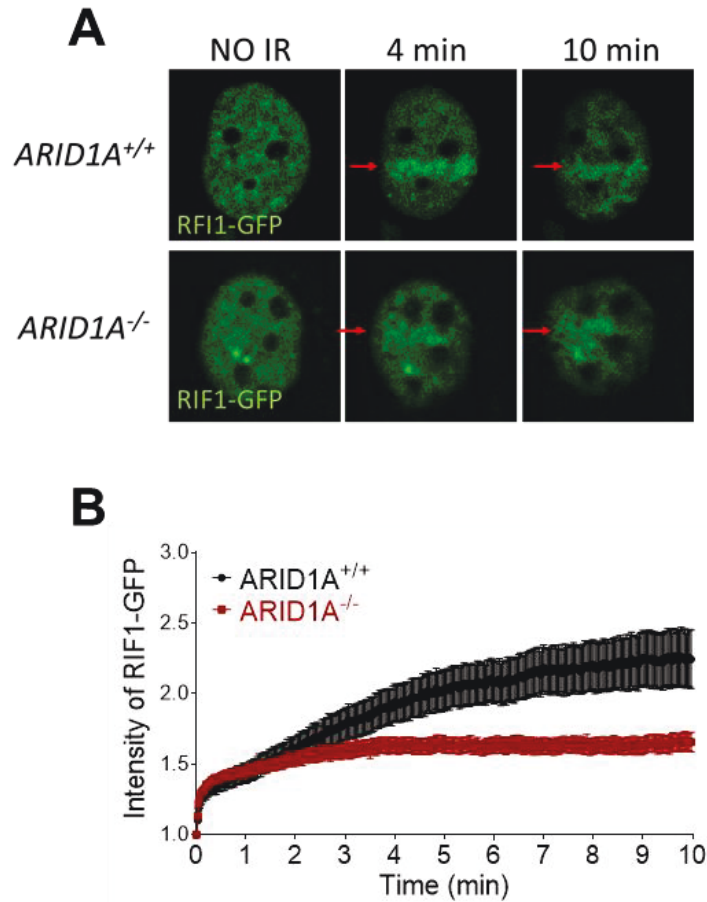
Figure 2-17. Quantification of RIF1 recruitment at the DSB sties. (A) Representative live images of hEM cells transfected with RFI1-GFP were shown at the indicated time points after microirradiation (red arrow). (B) The GFP intensity at irradiated area (yellow box) was measured and plotted as described above. Data was presented as a mean ± SEM, n>12
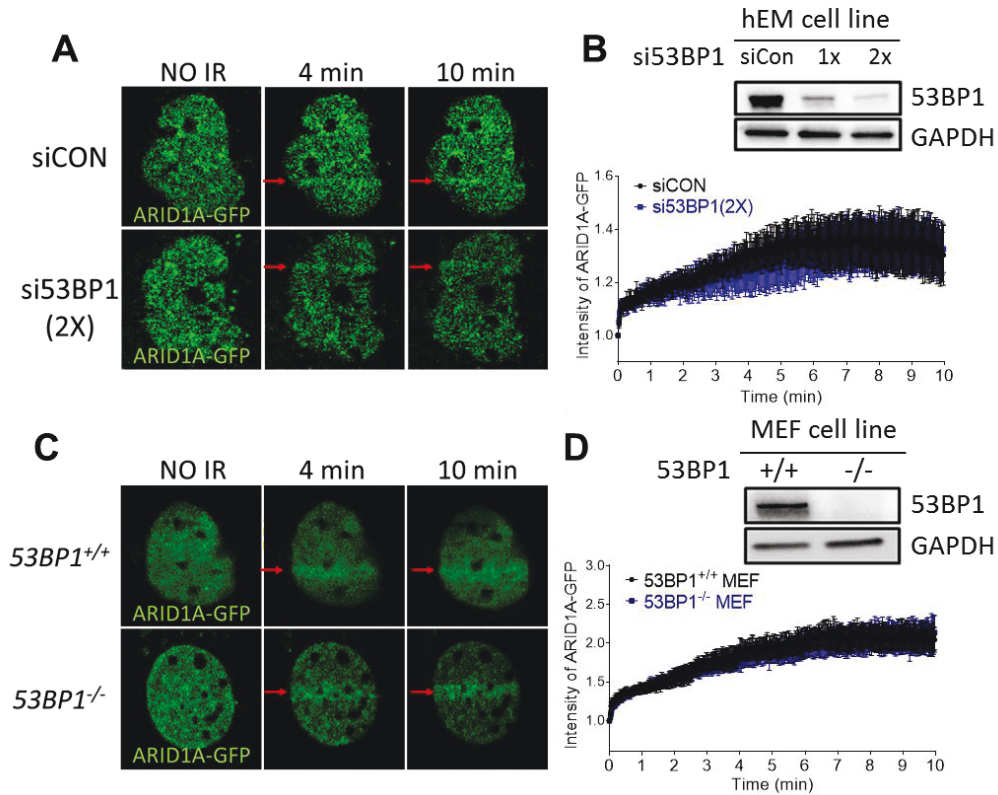
Figure 2-18. Quantification of ARID1A recruitment at the DSB sites. (A) Representative live images of hEM cells were shown. Cells were transfected with indicated siRNAs twice (2x), and seeded for 24 hours. Then, cells were transfected with ARID1A-GFP and microirradiated (red arrow). (B) The GFP intensity at irradiated area (yellow box) was measured and plotted as described above. Immunoblotting analysis showed levels of 53BP1 and GAPDH was used as a loading control. Data was presented as a mean ± SEM, n>4 (C) Representative live images of MEF cells were shown. Cells were transfected with ARID1A-GFP and microirradiated (red arrow). (D) The GFP intensity at irradiated area (yellow box) was measured and plotted as described above. Immunoblotting analysis showed levels of 53BP1 and GAPDH was used as a loading control. Data was presented as a mean ± SEM, n>5

47

Chapter 3. The Effects of Targeted Therapy

in ARID1A Mutated Cancers

3-1. PARP inhibition and radiation are synergistically cytotoxic to ARID1A deficient cells.

While ARID1A deficient cells showed increased sensitivity to radiation-induced cell death, the high doses of radiation required for eliciting tumor regression *in vivo* are often associated with significant side-effects in the clinical setting. The development of radiosensitizing agents to maximize therapeutic index while minimizing side-effects is therefore of clinical importance. To address this issue, we tested a panel of compounds to find potential radiosensitizers specifically targeting ARID1A deficient cells (**Figure 3-1**). Our screening panel included conventional chemotherapeutic drugs, including carboplatin, paclitaxel, doxorubicin and camptothecin; inhibitors of DNA repair proteins, such as PARP, ATR, ATM and Chk1; and drugs targeting epigenetic regulators, including HDAC and EZH2 inhibitors. ARID1A$^{+/+}$ and ARIDA$^{-/-}$ hEM3 cells were treated with low-doses of radiation, combined with the varying concentrations of the tested compound; synergism was determined using the Combination Index (CI).

Among the tested drugs, the PARP inhibitor, Olaparib, demonstrated the strongest synergism with radiation treatment, specifically towards ARIDA$^{-/-}$ cells. In a 3-D culture system, which more closely recapitulates human tumors *in vivo*, combined radiation and PARP inhibition (IR+PARPi) was also more effective in killing ARID1A$^{-/-}$ hEM3 and MCF10A cells, compared to ARID1A$^{+/+}$ controls (**Figure 3-2**).

To gain insight into the underlying processes responsible for the increased sensitivity of ARID1A$^{-/-}$ cells to PARPi+IR, levels of γH2AX were assessed by western blotting of lysates from ARID1A$^{+/+}$ and ARID1A$^{-/-}$ cells following IR, PARPi or combined

treatment (**Figure 3-3**). IR treatment resulted in the accumulation of γH2AX, which was more marked in ARID1A$^{-/-}$ (3-fold increase over baseline, untreated condition) compared to ARID1A$^{+/+}$ cells (2-fold increase). Notably, while PARPi+IR did not cause any further changes in γH2AX in ARID1A$^{+/+}$ cells over single-agent treatment, a dramatic 7-fold increase was observed in ARID1A$^{-/-}$ cells. The correlation between γH2AX and cell viability following treatment suggests that the massive accumulation of unrepaired DNA DSBs underlies the synthetic lethality of PARPi+IR when ARID1A is lost.

PARP inhibitors are thought to generate DSBs through two major mechanisms. First, olaparib binds to the NAD+ binding pocket of PARP proteins, blocking PARylation, which is an important requirement for PARP to dissociate from DNA. This 'PARP-trapping' interferes with DNA replication, and leads to DSB. The other possibility is that inhibition of PARP results in the persistence of single-strand breaks, which ultimately progress to DSBs. To determine which of these processes are relevant in our model system, we deleted PARP1 by CRISPR in hEM3 cells isogenic for ARID1A. As the effects of genetic knockout of PARP1 were similar to inhibition by olaparib, we conclude that loss of the PARP-mediated repair is the main source of DSBs, since PARP-trapping cannot occur in the absence of PARP (i.e. knockout).
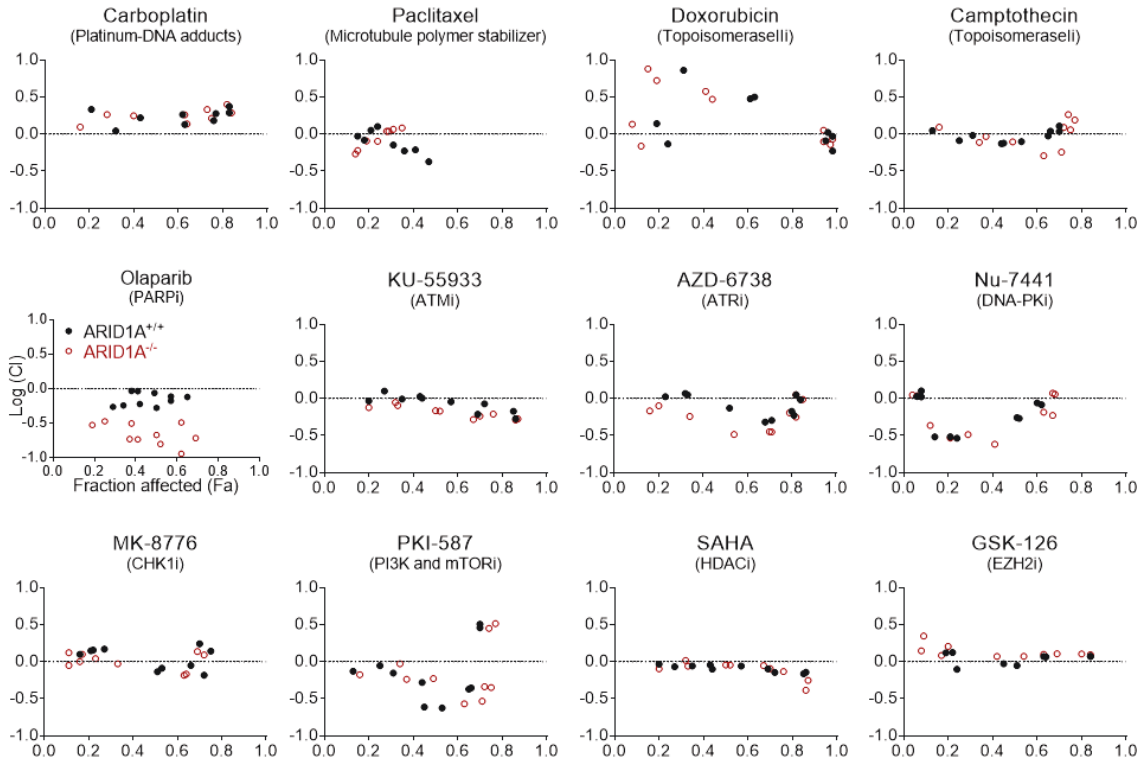
Figure 3-1. Combination index of irradiation and inhibitors. Logarithmic combination index (CI) plot of irradiation (1Gy and 2Gy) is generated in combination with indicated drugs (series of concentrations) in hEM cells. Cell viability was measured at day 3 of treatment and CI was calculated using CompuSyn software. The horizontal dash lines at Log (CI)=0 were drawn for discrimination of synergism [Log (CI)<0] and antagonism [Log(CI)>0].
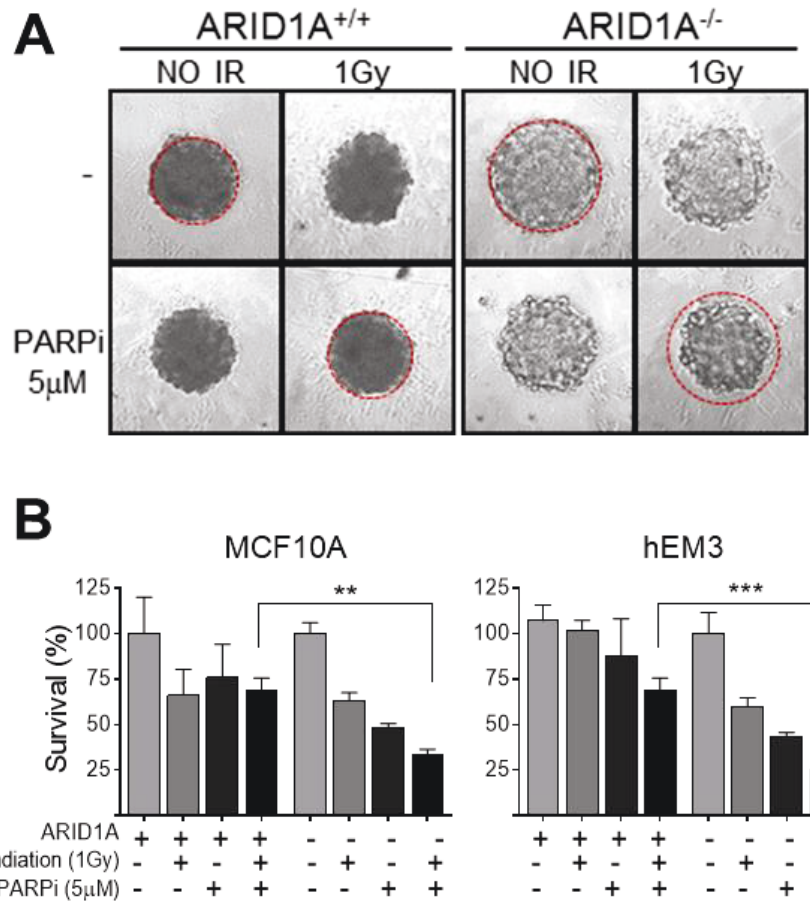
Figure 3-2. Cell viability after single or combined treatments in 3D culture system.

(A) Representative live MCF cells in 3D hanging drop system were shown. After spheroids were formed, cells were treated with indicated treatments and cell viability was measured at day 4. The yellow dash lines were drawn for comparing cell spheroid size between control and treatment groups. Data was presented as a mean ± SEM, n>3, * p<0.05, ** p<0.01, *** p<0.001
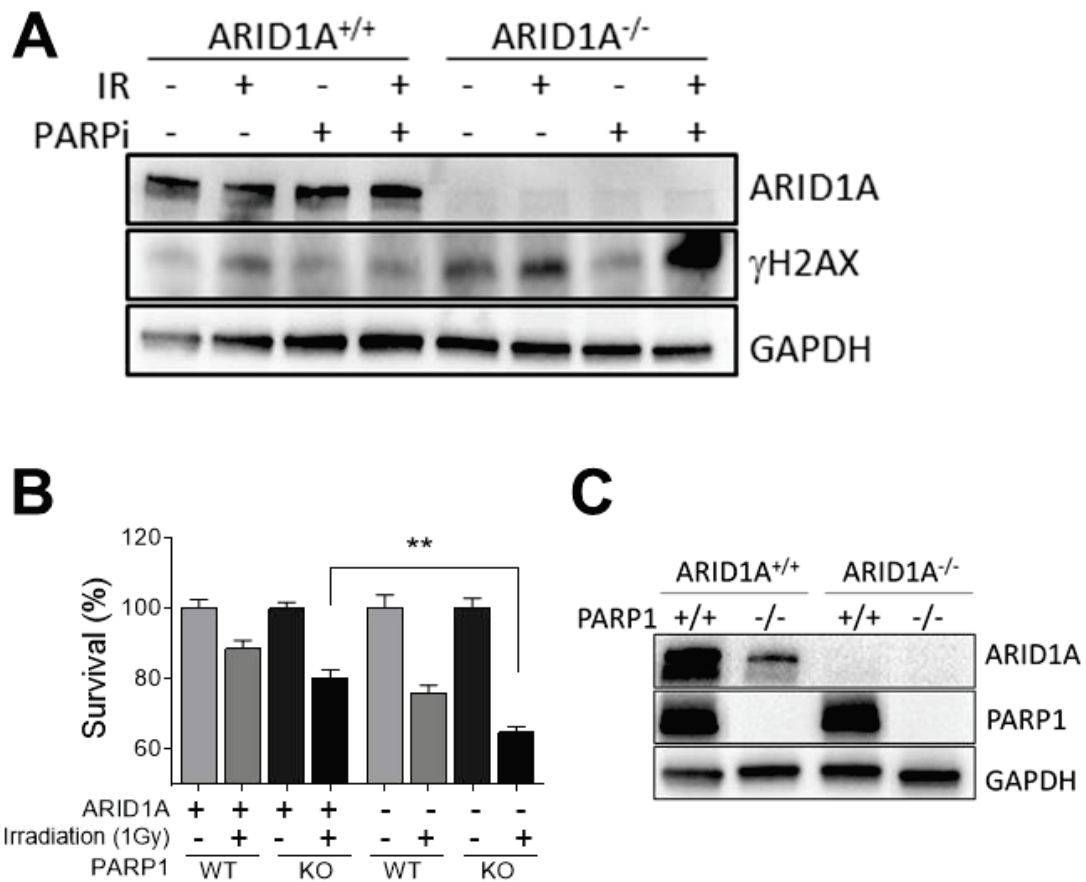
Figure 3-3. Quantification of γH2AX after single or combined treatments. (A) Immunoblotting analysis showed levels of ARID1A and γH2AX in hEM cells after indicated treatment. GAPDH was used as a loading control. (B) Cell viability was measured after irradiation treatment. (C) Immunoblotting analysis showed levels of ARID1A and PARP1 in hEM ARID1A/PARP1 double knockout cells. GAPDH was used as a loading control.

3-2. Combining PARP inhibitor with radiation is more effective than single-agent therapy in ARID1A-mutated tumors *in vivo*

Given the synergistic effects of combining olaparib with irradiation in ARID1A$^{-/-}$ cells *in vitro*, we proceeded to preclinical evaluation of this treatment strategy in animal models. The HCT116 isogenic pair was used to establish xenografts in nude mice; ARID1A$^{+/+}$ and ARID1A$^{-/-}$ cells were injected subcutaneously into the right and left flank, respectively (**Figure 3-4**). Mice were randomly stratified into four treatment groups: 1. Control - No treatment, 2. radiation (IR; 1.5 Gy), 3. Olaparib (PARPi; 50mg/kg by intraperitoneal injection), or 4. PARPi followed by IR two hours later, (PARPi+IR) (**Figure 3-5**). We checked the PARP inhibitor effectively reduces PARP activity by measure PARylation in our mouse model, and CT-guided irradiation machine specifically target tumors by measuring γH2AX. Furthermore, we could not observe weight loss of abnormal behavior throughout treatment. Treatments were administered every other day, starting when tumor size reaches more than 150mm, and tumor size was monitored over 2 weeks.

Strikingly, PARPi+IR completely prevented the growth of ARID1A$^{-/-}$ tumors and demonstrated superior efficacy over PARPi or IR alone (**Figure 3-6**). In contrast, for the contralateral ARID1A$^{+/+}$ tumors, the addition of PARPi to IR did not result in further reductions in tumor growth, which continued to progress insidiously over the course of the experiment. Similar results were obtained in xenograft models of two endometrial carcinoma cell lines (ECC1 (ARID1A-wildtype), HEC151 (ARID1A-mutant)), and two

clear cell carcinoma cell lines (RMG1 (ARID1A-wildtype), TOV21G (ARID1A-mutant)), extending the generalizability of our findings (**Figure 3-7**).

Since patients are not treated indefinitely in the clinical setting, we sought to determine the prognostic outcome after discontinuation of treatment. Using the bilateral HCT116 isogenic pair model, mice were treated with PARPi followed by radiation (2 Gy) every other day until Day 25 (**Figure 3-8**). Monitoring of tumor size over time revealed rapid regrowth of ARID1A$^{+/+}$ tumors following cessation of therapy, while ARID1A$^{-/-}$ tumors never recovered and in fact, continued to shrink. Furthermore, one mice had complete remission.

To evaluate the apoptosis in the xenograft tumors, we measured cleave-caspase 3 intensity in each tumor after 2weeks combination treatment. (**Figure 3-9**). In the same tissue, we found that the level of DSBs, presented as γH2AX, was much higher in ARID1A$^{-/-}$ compared to ARID1A$^{+/+}$, suggesting increased DSBs cause cell apoptosis. In concordance with tumor shrink result, we checked the level of cleaved-caspase 3, cleaved-PARP1 as well as annexin V positive in HCT116 cells after combination treatment, and concluded that ARID1A deficiency increases apoptosis in respond to the combination treatment of PARP inhibitor and irradiation.

Collectively, the data provide a rational basis for combining PARP inhibition with radiation therapy for the treatment of ARID1A mutant cancers; the sudden overload of DSBs generated by combined radiation and PARP inhibition cannot be repaired by ARID1A deficient cells.
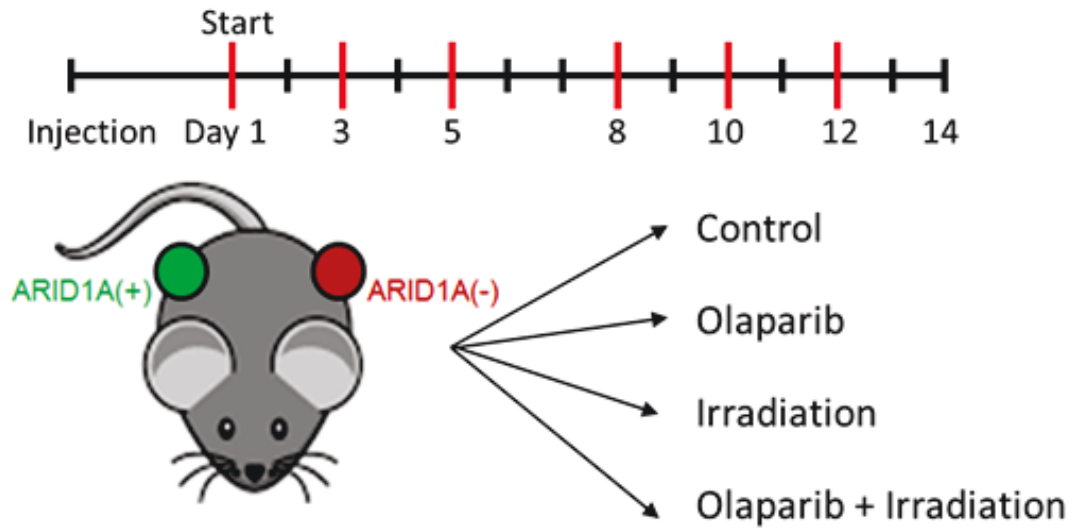
Figure 3-4. Schematic representation of animal treatment schedule. Xenografts were established with ARID1A$^{+/+}$ or ARID1A$^{-/-}$ tumor cells into the right and left flank by subcutaneous injection in athymic nu/nu mice. Mice were randomly divided into 4 groups; control, olaparib, irradiation and combination. Treatments were administered every other day, starting when tumor size reaches more than 150mm, and tumor size was monitored over 2 weeks.
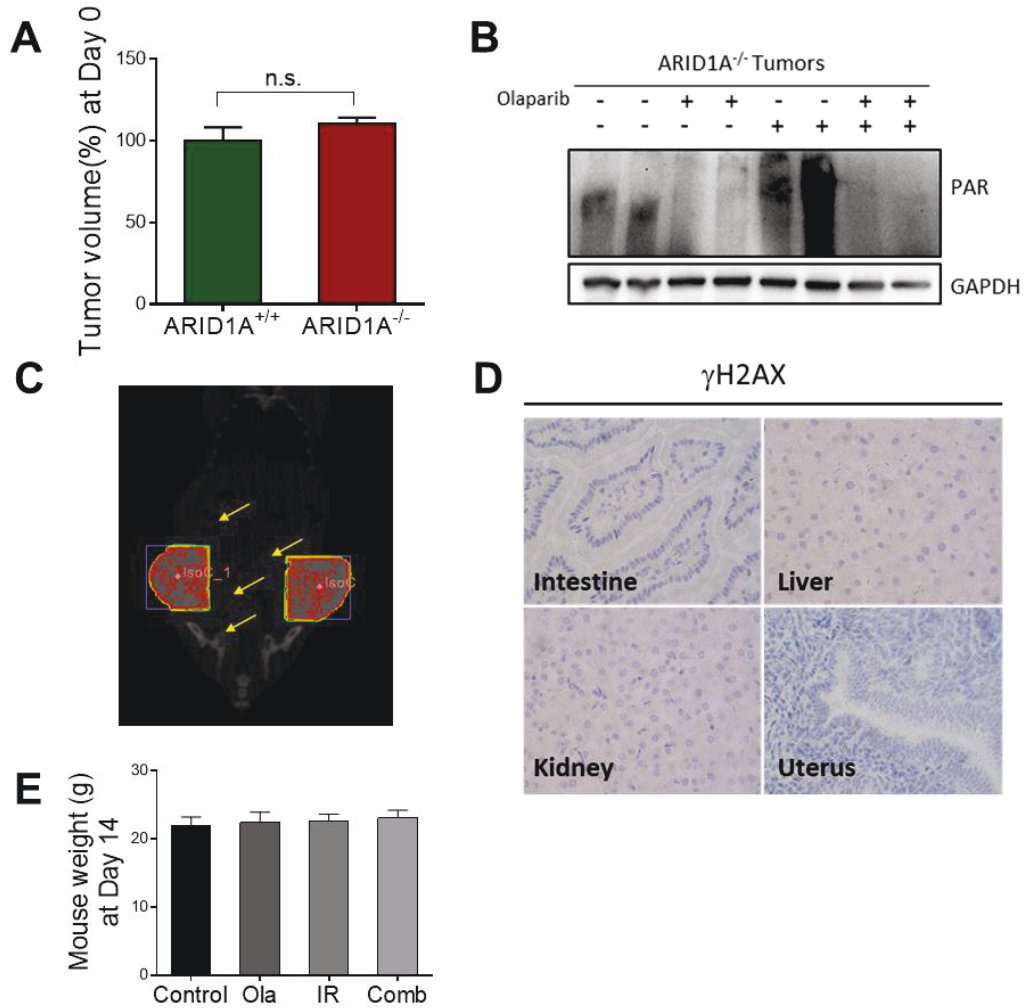
Figure 3-5. Verification of animal treatment conditions. (A) The average size of tumors with HCT116 ARID1A^{+/+} (green) and ARID1A^{-/-} (red) at Day 1 was plotted. (B) Immunoblotting analysis showed the level of PAR (Poly-ADP ribosylation) from tumors with indicated treatments. (C-D) Representative image of targeting tumors with Small Animal Radiation Research Platform (SARRP). Targeted areas were shown as red. Non-targeted areas marked as yellow arrows presented no DNA damaged by staining with anti-γH2AX. (E) Average of mouse weight was plotted as indicated.
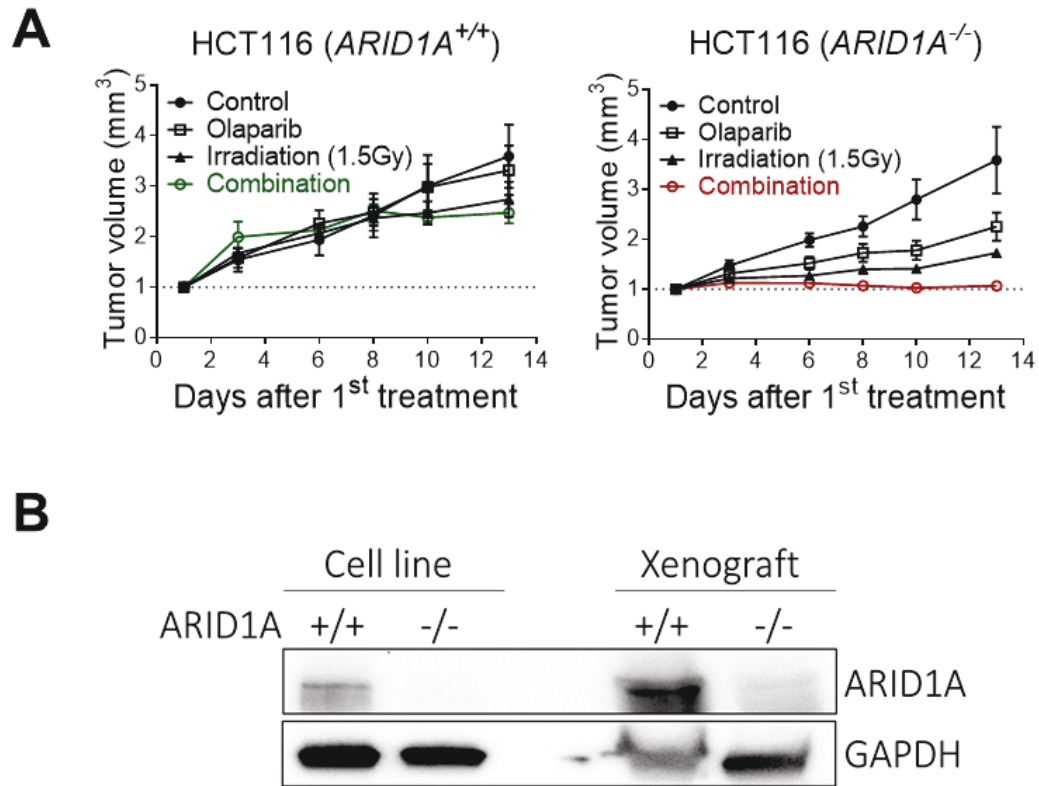
Figure 3-6. HCT116 xenografts growth after single or combined treatments. (A) Average tumor volume [(width)^2 x length/2] of each group was determined at the end of the scheduled treatment and plotted. Tumor volume from combination treatment group were presented as green (ARID1A$^{+/+}$) or red (ARID1A$^{-/-}$). (n>5, IR 1.5Gy, Olaparib 50mg/kg) (B) Immunoblotting analysis showed levels of ARID1A and GAPDH (control) in from HCT116 cell line and xenografts.
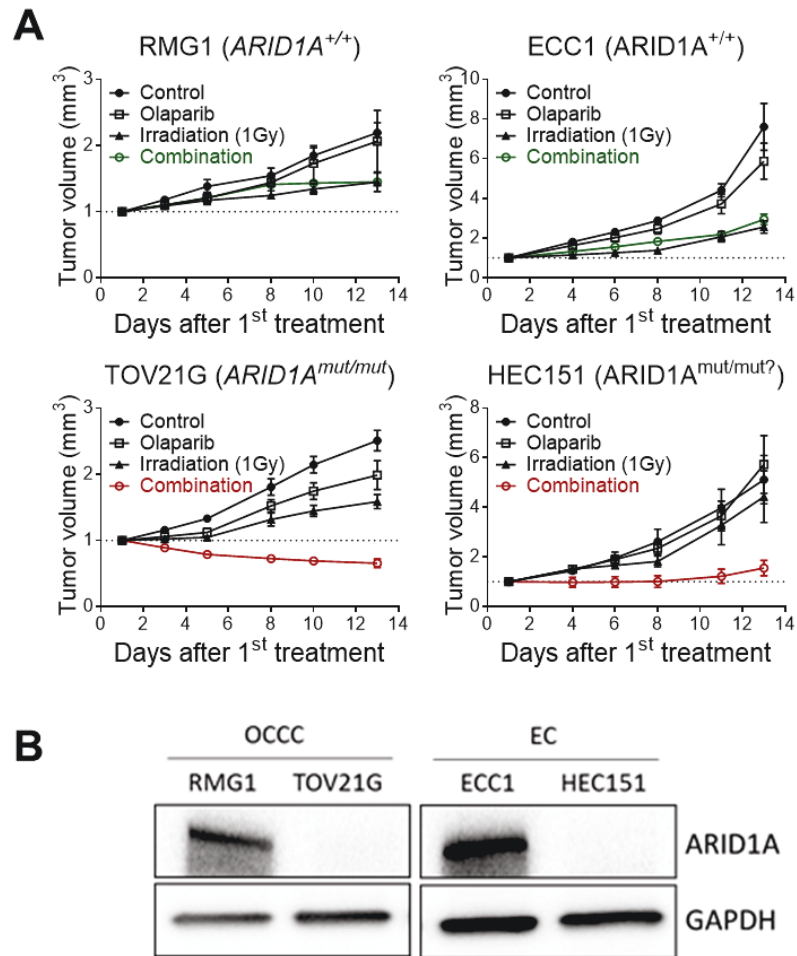
Figure 3-7. Xenografts growth with RMG1, ECC1, TOV21G1 and HEC15 cells after treatments. (A) Xenografts were established with two endometrial carcinoma cell lines [ECC1 (ARID1A-wildtype), HEC151 (ARID1A-mutant)], and two clear cell carcinoma cell lines [RMG1 (ARID1A-wildtype), TOV21G (ARID1A-mutant)]. Average tumor volume [(width)^2 x length/2] of each group was determined at the end of the scheduled treatment and plotted. Tumor volume from combination treatment group were presented as green (ARID1A$^{+/+}$) or red (ARID1A$^{-/-}$). (n>6, IR 1Gy, Olaparib 50mg/kg) (B) Immunoblotting analysis showed levels of ARID1A and GAPDH (control) in indicated cell lines.
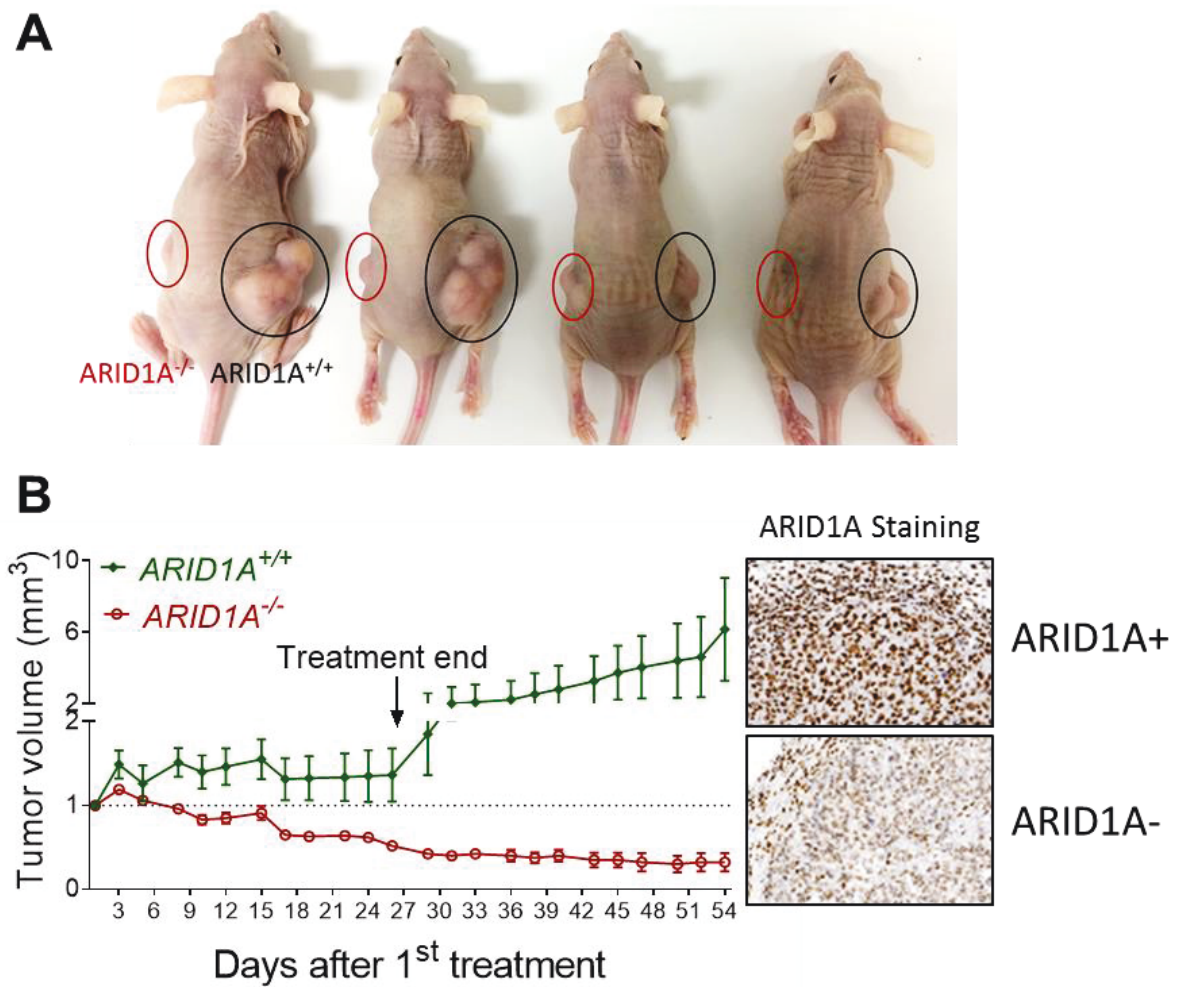
Figure 3-8. Tumor growth following cessation of combination treatment. (A) Representative image of xenografts bearing mice were shown at the Day 54. (B) Average tumor volume [(width)^2 x length/2] of combination group was presented. Treatment was stopped at Day 27, and tumor volume was monitored without treatment until Day 54. (n=4, IR 2Gy, Olaparib 50mg/kg) (B) Representative examples of the immunohistochemistry analyses of xenograft tumors with anti-ARID1A were presented.
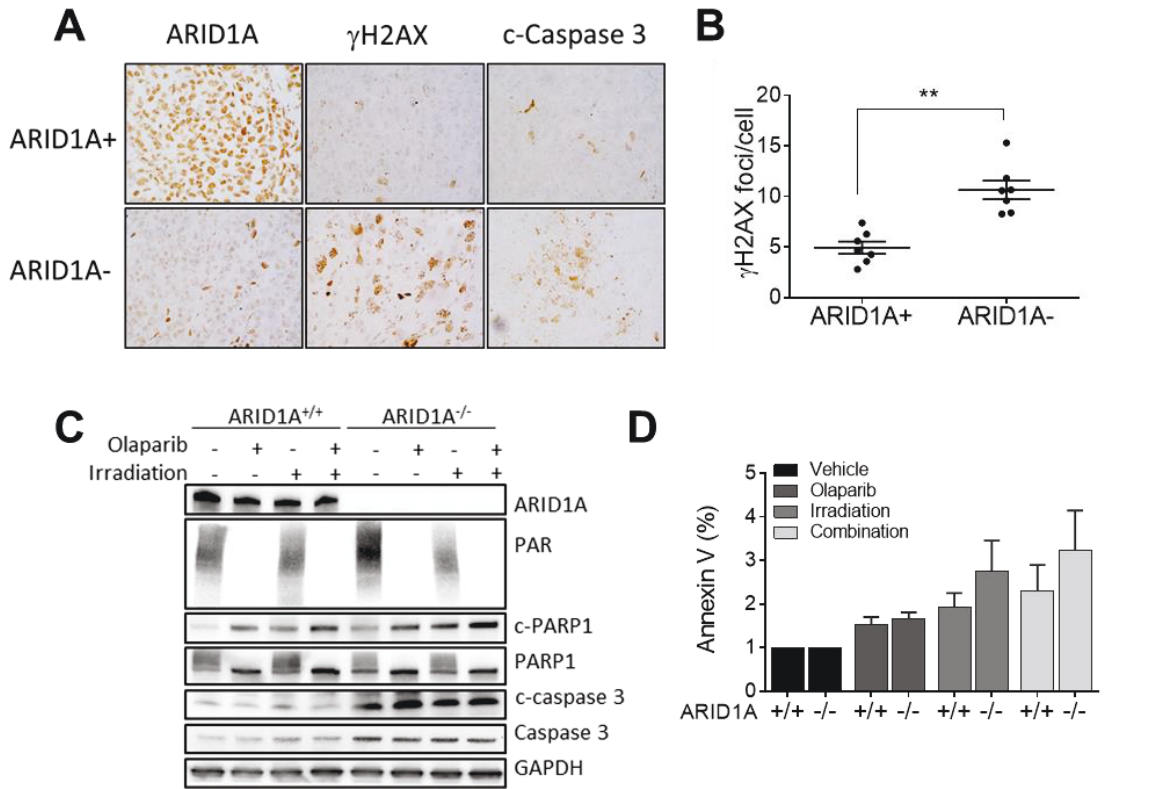
Figure 3-9. Quantification of DSBs and apoptosis after single or combined treatments.

(A) Representative examples of the immunohistochemistry analyses of xenograft tumors in combination group with anti-ARID1A, γH2AX and cleaved-caspase 3 were presented. (B) Quantitation of γH2AX foci was shown. Data was represented as a mean ± SEM, n>100. n>15. * p<0.05, ** p<0.01, *** p<0.001 (C) Immunoblotting analysis showed levels of ARID1A, PAR, cleaved-PARP1, PARP1, cleaved-caspase3, caspase3 and GAPDH (control) in HCT116 cells after indicated treatment. (D) Quantification of annexin V-positive cells was performed using an annexin V/PI kit. Percentage of HCT116 cell apoptosis (flow cytometry) after each treatment was plotted

Chapter 4. Discussion

Discussion

Based on their clinical behaviour and molecular features, a dualistic model for the classification of endometrial and ovarian carcinomas has been proposed. Type I tumors are traditionally described as indolent, localized and low-grade, and include the endometrioid and clear cell histologic subtypes (despite the more aggressive nature of the latter), while the Type II tumors, consist of high-grade serous carcinomas, which exhibit rapid progression, are widely metastatic and cytologically high-grade. Genomic sequencing studies have revealed subtype-specific molecular genetic alterations and are in support of the dichotomous categorization. High-grade serous carcinoma is characterized by p53 mutations and widespread copy number alterations. In contrast, endometrioid and clear cell carcinomas harbour frequent mutations in ARID1A, mutations causing activation of the PI3K pathway, defective mismatch repair and a relatively quiescent genomic copy number profile.

There is accumulating evidence that the dualistic classification can be extended to describe response to different types of treatment. High-grade serous carcinoma is sensitive to platinum-based chemotherapy, particularly those with defective HR (up to 50% of cases). In contrast, reports of subtype-specific differences in response to RT have demonstrated better clinical outcomes in endometrioid tumors in one study[110], and for Stage I ovarian carcinomas, non-serous (i.e. endometrioid, clear cell and mucinous) subtypes were more likely than to be cured by RT than serous carcinoma. The commonly accepted explanation for this phenomenon relates to the extent of dissemination; endometrioid and clear cell tumors tend to be localized, while serous carcinomas disseminate widely in the peritoneal

cavity. An intriguing possibility is that the subtype-specific sensitivity to RT might also be explained, at least in part, by the differential functional capacity of NHEJ across tumor types.

NHEJ is the primary mechanism for the repair of DSBs during G0 and G1 phases, while DSBs generated during S and G2 phases are repaired by HR. Therefore, while impaired chromatin remodelling in response to DNA damage causes a general impairment in accessibility of chromatin to repair machinery, as demonstrated by the traffic-light reporter assay, in most cells (i.e. in G0 and G1), it is NHEJ that is impacted upon irradiation. Furthermore, whereas high-grade serous carcinomas are highly proliferative, the proliferative index of endometrioid and clear cell carcinomas is significantly lower, consistent with a larger abundance of tumor cells in G1. Since NHEJ is the main repair mechanism for radiation-induced DNA damage, ARID1A-mutant endometrioid and clear cell tumors are therefore more sensitive to RT than high grade serous carcinomas, in which NHEJ is typically fully functional.

Our search for small molecule compounds that further sensitize ARID1A$^{-/-}$ cells to irradiation surprisingly identified the PARP inhibitor, olaparib. While the synthetic lethality of PARP inhibition in HR-defective serous ovarian carcinomas is widely accepted, this is the first report demonstrating its potential use as a radiosensitizing agent targeting ARID1A-mutated tumors in a selective manner. While the exact mechanism remains to be elucidated in a future study, our initial investigations have provided some clues.

Since loss of ARID1A is associated with a global increase in PARylated proteins, it is likely that hyperactivity of PARP1, responsible for 90% of cellular PARylation events[59], acts as a compensatory mechanism to alleviate the basally elevated genotoxic stress in these cells. It is possible that PARylation, being a negatively-charged modification, facilitates chromatin relaxation by charge repulsion of DNA (also negatively charged) and recent work has suggested that PARP1 is involved in chromatin relaxation. PARylation is also known to serve a scaffolding function for recruitment of other chromatin remodelling enzymes, including ALC1[111], and DNA repair complexes.

PARP1 hyperactivation has also been reported in HR deficient cells, though it is unclear why PARP1 inhibition alone can kill HR deficient serous carcinomas, but exert only minimal effects on ARID1A-mutated tumor cells. As the enhanced cytotoxicity of PARP1 inhibition can only observed with radiation exposure, the relationship between PARP1 and ARID1A may be appropriately described as 'conditional' synthetic lethality, as opposed to the *bona fide* synthetically lethal interaction between PARP1 and BRCA1/2. Perhaps, in the case of serous carcinoma, increased chromosomal instability and the endogenous source of DSBs from replication stress may preclude the necessity of an external source of DSBs. Also while the trapping of PARP1 to damaged DNA by olaparib has been demonstrated in HR deficient models, we show that genetic knockout of PARP1 also sensitized ARID1A$^{-/-}$ cells to irradiation, suggesting that trapping of PARP does not play a significant role in radiosensitization.

There was, however, a modest increase in the number of cells with small insertions/deletions, indicative of alternative-NHEJ-mediated repair, (a process recently

shown to involve PARP1 function), in irradiated ARID1A$^{-/-}$ cells (**Figure 4-1**). Moreover, the inhibition of Ligase-3, which functions exclusively in alternative-NHEJ, also sensitized ARID1A$^{-/-}$ cells (**Figure 4-2**). Future studies should investigate the role of alternative-NHEJ as a compensatory repair mechanism in the context of ARID1A-deficiency and its relative importance in explaining PARP inhibition-radiation synergy. Regardless, the accumulation of unrepaired DSBs, reflected by dramatic increases in levels of γH2AX following combination olaparib with RT treatment, exceeding the tolerable threshold, is likely a major factor in eliciting tumor cell death.

A recent Phase I clinical trial has demonstrated the safety and tolerability of combining PARP inhibitor with low-dose fractionated whole abdominal radiation therapy in the treatment of metastatic cancers with peritoneal dissemination. Stratification of patients by molecular features, including ARID1A mutation, may potentially select those most likely to respond to this therapeutic approach.

In summary, our data highlight the suppression of the chromatin relaxation response to DNA DSB upon loss of ARID1A, with the most profound consequences observed in NHEJ-mediated repair. The increased sensitivity of ARID1A-mutant tumors to radiation, which could be amplified by concurrent PARP inhibition, warrants clinical validation. The present study adds to the body of evidence supporting the dualistic classification of gynaecologic cancers, suggesting that it could potentially be extended to rationally select patients for specific therapies, namely platinum-based chemotherapy and/or PARP inhibitor for Type II tumors and radiation with/without PARP inhibitor for Type I tumors.

66

A TALEN System / CRISPR System

B
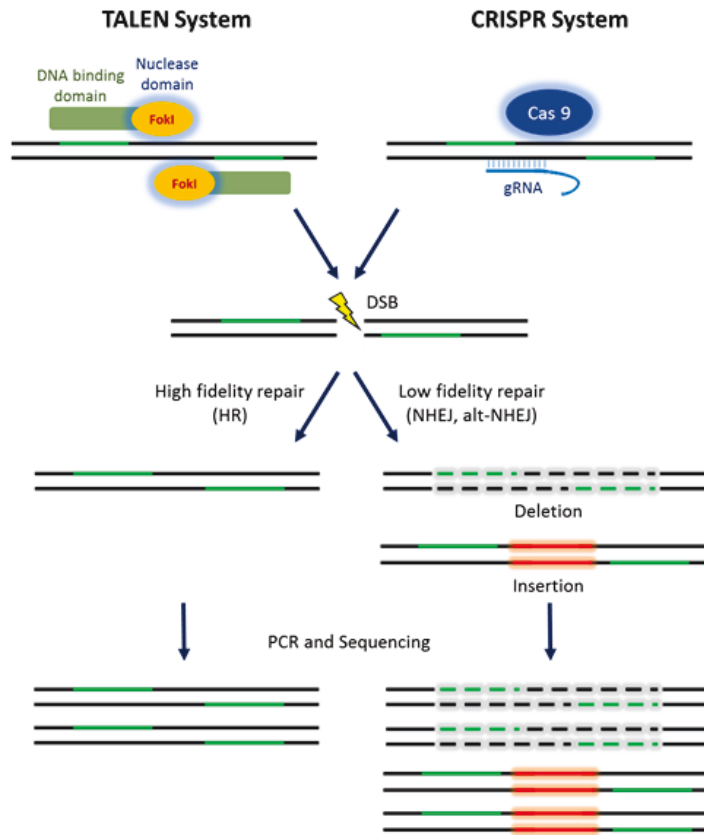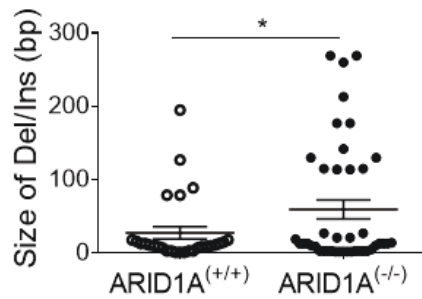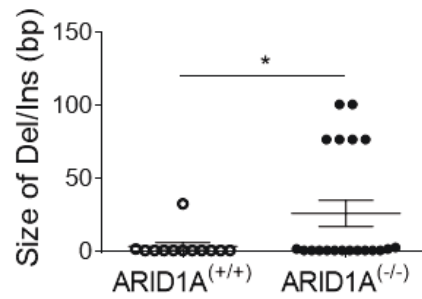
Mutation Size (bp)	Mutation / total colonies (rate)	
	ARID1A^{+/+}	ARID1A^{-/-}
>30	5/69 (7.24%)	16/92 (17.4%)
16-30	3/69 (4.3%)	4/92 (4.3%)
2-15	17/69 (24.6%)	19/92 (20.7%)
1	3/69 (4.3%)	0/92 (0%)
0	48/69 (69.6%)	69/92 (75%)

C

Mutation Size (bp)	Mutation / total colonies (rate)	
	ARID1A^{+/+}	ARID1A^{-/-}
>30	1/101 (1%)	5/116 (5.2%)
16-30	0/101 (0%)	0/116 (0%)
2-15	1/101 (1%)	3/116 (2.6%)
1	10/101 (9.9%)	11/116 (9.5%)
0	89/101 (88.1%)	96/116 (82.8%)

67

Figure 4-1. Experimental scheme and analysis of junction of DSBs. (A) Experimental scheme of sequencing at the junction of DSB repair. HCT116 (B), MCF10A and hEM3 (C) cells were transfected with AAVS1-specific TALEN (B) or AAVS1-specific CRISPR/Cas9 (C) nucleases. After 24 hours, genomic DNA was extracted and AAVS1 region was amplified by PCR. The PCR products were sequenced followed by TOPO TA cloning. All insertions or deletions from ARID1A WT and deficient cells was presented on the graph. Frequency of insertions or deletions with changes of more than 35bp was presented as a table. * $p<0.05$, ** $p<0.01$, *** $p<0.001$
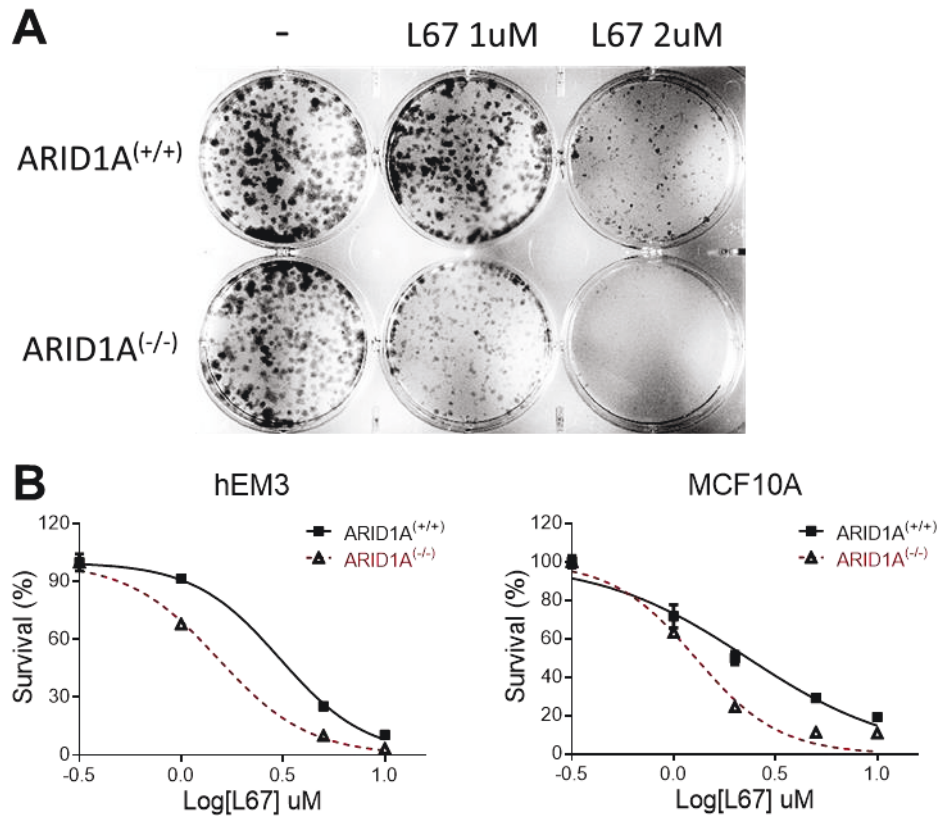
Figure 4-2. Cell survival after ligase 3 inhibitor (L67) treatment. (A) Representative images of the colony forming assay were presented. 1×10^4 of hEM3 cells were seeded for 24 hours and treated with various doses of L67. Colonies were visualized with crystal violet on day 5. * $p<0.05$, ** $p<0.01$, *** $p<0.001$ (B) Cell survive curves for hEM3 and MCF10A cells were presented. 1×10^3 of cells were seeded for 24 hours and treated with various doses of L67. Cell viability was measured by cell titer blue on day 4. Data was presented as a mean ± SEM of triplicates.

Chapter 5. Material and Methods

5-1. Mouse model and xenograft

All animal studies and procedures were approved by the Johns Hopkins Animal Care and Use Committees. PAX8-rtTA/TetO-Cre strains (C57Bl background) were acquired from the Dr. Ronny Drapkin[112]. Arid1a$^{flox/flox}$ mice on the C57BL/6 background was previously described. Both mice were bred to obtain homozygous Arid1a-Pax8/Cre (APC) mice with genotyping procedures are as described previously.[49,112] In order to drive Cre-mediated recombination in murine uterine epithelial cells, we treated experimental and control mice for 7 days with doxycycline using oral gavage. Animals were routinely monitored for signs of distress, poor body condition, and tumor burden and were euthanized according to veterinary recommendations. For xenografts assay, 2×10^6 of cells were injected with matrigel (v/v) (BD Biosciences) into the subcutaneous tissue on the right and left flanks of 5-6 weeks old nu/nu mice. Approximately 2 weeks after inoculation, when tumor volume reaches >150mm, mice were randomized into different group and received treatment. Tumors were excised at the end of experiment and fixed in 10% buffered formalin and embedded in paraffin.

5-2. Cell culture and plasmids

The normal endometrial epithelial cell line, hEM3, was established from human endometrium and characterized in our lab. hEM3 cells were cultured in RPMI 1640 with 15% FBS and 1% penicillin and streptomycin (P/S), supplemented with 10mM HEPES, 1x non-essential amino acids, 2μg/mL insulin, 200ng/mL endothelial growth factor, and 100nM estradiol. Two pairs of isogeneic cell lines, HCT116 and MCF10A, were purchased from Horizon Discovery Ltd. Each pair consisted of parental and ARID1A homozygous

knockout cell lines and were cultured according to the manufacturer's instructions. ARID1A inducible cancer cell lines, OVISE and HEC1A, and other cancer cell lines (TOV21G1, RMG1, HEC151, ECC1) were grown in RPMI 1640 or DMEM with 10% fetal bovine serum (FBS), and 1x (P/S). ARID1A-knocked-out hEM3 cells were generated previously as described.[54] All cells were incubated at 37°C with 5% CO2. Control siRNA (12935200) and two ARID1A specific siRNAs (HSS112109, HSS112110) were purchased from Life Technologies (Waltham, MA). BRCA1 specific siRNA for BRCA1 (SI02664368) and CtIP (sc-37765) was obtained from Qiagen (Hilden, Germany) and santa cruz biotechnology (Dallas, TX). The sequence of si53BP1 is 5'-CACACAGAUUGAGGAUACG-3'. The EGFP-ARID1A was a from Dr. Guang Peng (The University of Texas MD Anderson Cancer Center). pCVL Traffic Light Reporter 1.1 (Sce target) (Plasmid #31482), pCVL SFFV d14GFP (Plasmid #31476), 53BP1-GFP (Plasmid #60813) and RIF1-GFP (Plasmid #52506) were purchased from Addgene. 53BP1-mCherry was generated from MRC PPU Reagents and Services (Dundee, Scotland).

5-3. Antibodies and reagents

Anti-p-ATM (S1981) (1:1000), γH2AX (S139) (1:2000), GAPDH (1:2000), PARP1 (1:2000), Histone 2B (1:2000), cleaved Caspase-3 (1:1000) and anti-rabbit IgG Alexa Fluor 488 Conjugate were purchased from Cell Signaling Technology. Anti-pATM (S1981) (1:1000), GFP (1:200) and pKAP1 (S824) (1:1000) were from Abcam (Cambridge, United Kingdom) and Bethyl Laboratories (Montgomery, TX). Anti-ARID1A (1:2000) was purchased from Sigma and 53BP1 (1:2000) antibody was obtained from Novus (Littleton, CO). Carboplatin was purchased from Sigma and GSK126 was obtained from Xcess

Biosciences and Active Biochem. L67 was from Medchem express (Monmouth Junction, NJ). All other drugs and small inhibitors were from Selleckchem (Houston, TX). The Estradiol, Cholera Toxin, and Gelatin from porcine skin were purchased from Sigma-Aldrich (St. Louis, MO). Epidermal growth factor was purchased from BD Biosciences (San Jose, CA), and Insulin and Human Recombinant Zinc Solution were from Invitrogen (Carlsbad, CA). Trypsin-EDTA, HEPES buffer, MEM Non-Essential Amino Acids Solution, PBS, RPMI, FBS, and Penicillin/Streptomycin were also purchased from Invitrogen.

5-4. Laser microirradiation assay

Cells were seeded in nunc glass bottom dish (Thermo Scientific) and transfected with a GFP-ARIDIA or GFP-53BP1 or mCherry-53BP1 or GFP-RIF1 plasmid (2μg) with lipofectamin 3000. Eight to twenty-four hours later, cells were incubated with 2μg/ml Hoechst (Thermo Scientific) for 10 min and mounted on a preheated (37C) stage on a Zeiss LSM 710 confocal microscope equipped with 405 nm laser source. A region of the cell nucleus was irradiated and the images were taken at 3 second intervals to detect recruitments or replacement of the GFP or mCherry-tagged proteins to the site of damage (red arrow). To induce localized DSBs, the laser setting was set to 100% power output with 4 laser iterations. For reduced laser, we used 405nm laser at 40% power output with 2 laser iterations. The kinetics were calculated using Zeiss Zen 2010 software.

5-5. Immunohistochemistry

Paraffin-embedded mouse liver tissue was deparaffinized in xylene and rehydrated in alcohol. Antigen retrieval was performed with Trilogy (Cell Marque), and endogenous

peroxidase activity was blocked by incubation using 1% H_2O_2 in methanol for 15 min. Tissues were blocked with blocking solution (Dako Antibody diluent) for 30 min, and incubated with primary antibodies in Dako Antibody diluent at 4°C overnight. After washing with TBST (0.1% Tween 20) for 30 min, positive reactions were detected by applying EnVision+HRP polymer (Dako) for 30 minutes, followed by incubation in chromogen substrate for 5 minutes (Liquid DAB+; Dako). The slides were then counterstained with hematoxylin (Sigma,) and placed on a coverslip using Cytoseal (Thermo Scientific).

5-6. Cell viability and colony forming assay

1×10^3 cells were seeded in 96-well plates and treated with different doses of irradiation using a GammaCell40 irradiator equipped with a cesium-137 source at a rate of 52 cG/min. Four days after irradiation, cell viability was measured using Cell Titer Blue assay (Promega). According to the manufacturer's instructions, fluorescence was recorded at a 560/590-nm wavelength followed by 1 hour incubation. For the colony forming assay, 1×10^4 cells transfected with indicated RNAs and were seeded in 6 well plates, and irradiated 24 hours after seeding. At day 5, cells were stained with crystal violet (0.2% Crystal Violet, 3.7% PFA) for 10 minutes. After washing with dH2O, images were taken and analyzed with Image Lab™ (Bio Rad).

5-7. Cell comet assay

Neutral comet assay was performed to detect DNA DSBs by using Comet Assay Kit (Trevigen). After irradiation, cells were prepared according to the manufacturer's instructions. The images from all portions of the slide were randomly taken under a

fluorescence microscope. Tail moments were calculated by multiplying the tail intensity by length through the cell profiler, and subsequently analyzed by performing a student t-test using GraphPad Prism.

5-8. Western blot analysis

Protein lysates were prepared in cell lysis buffer (50mM Tris-HCl pH7.4, 150mM NaCl, 1% NP-40, 0.5% sodium deoxycholate). The extracts were electrophoresed on a 4–15% Mini-PROTEAN® TGX™ Precast Gel and then transferred to a PVDF membrane using the Trans-Blot® Turbo™ Transfer System (Bio Rad). After blocking with 5% non-fat dry milk (Fisher), the membrane was incubated with a primary antibody overnight at 4°C. The membrane was washed with TBST, and incubated with anti-rabbit or mouse IgG linked to HRP at RT for 1h. After short incubation with ECL solution (GE Healthcare, Pittsburgh, PA), signal was detected by ChemiDoc™ XRS+ System with Image Lab™ (Bio Rad). For extracting chromatin-bound proteins, we followed a subcellular protein fraction kit (Thermo Scientific).

5-9. Immunocytochemistry

Cover glasses were washed with 100% Ethanol and coated with 0.1% gelatin for 2 hours. Cells were seeded on top of the cover glasses, and 24 hours later cells were irradiated. Then, cells were fixed with 4% paraformaldehyde (Electron Microscopy Sciences, Hatfield, PA) for 10mi at RT, and incubated with 0.2% Triton X-100 (Sigma) in PBS for 10min. After blocking for 30 min with blocking solution (10% Normal goat serum (Cell Signaling), 0.3% triton X-100, 100mM Tris-Hcl [pH 7.5], and 150mM NaCl), cells were incubated with the primary antibody at RT for 1h. Then, cells were washed with PBS, incubated with Alexa-

Fluor-488 or 647 (1:200) for 1h at RT. Shortly after incubating cells with DAPI (Sigma, 50mg/ul, 1:5000), cover glasses were placed on slides using mounting solution (0.23 g DABCO (sigma), 8% H2O, 200mM Tris-Hcl, pH 8.0, 90% of Glycerol), and subsequently analyzed under a fluorescence microscope.

5-10. Traffic Light Reporter (TLR) assay

Lentiviral constructs coding for TLR were transfected into HEK293FT cells. After 8 hours, the supernatant of HEK293FT cells containing virus particles was collected, filtered and used for the transduction. To isolated TLR transfected cells (hEM3^{TLR}, HCT116^{TLR}), cells were incubated with puromycin (1μg/ml) for 5 days. The other lentiviral construct coding for I-Sce1 with donor e-GFP were generated as described above. Stable TLR transfected cells were transfected with siRNAs or not and 24 hours later transduced with donor lentiviral particles. Three days after transfection, cells were analyzed with LSRII (BD Biosciences). To measure eGFP (for HR repair) and mCherry signal (for NHEJ repair), 488 and 561-nm lasers were used for excitation, while 530/30 and 610/20 filters were used for the detection. Data were subsequently analyzed using FloJo software.

5-11. Combination index

Cells were seeded for 24 hours and treated with indicated drugs with various concentration 2 hours prior to irradiation (1Gy and 2Gy). Three days after, cell viability assay was performed and combination index was calculated. Synergistic drug interactions were analyzed using the Chou and Talalay method (Chou etal., 2003) based on the median-effect principle and the median effect equation: (fa)/(fu)=[(D)/(Dm)]m, where the ratio of the fraction affected (fa) over the fraction unaffected (fu) is equal to the dose (D) over the

median-effect dose (Dm) to the mth power, where Dm signifies potency and m signifies the sigmodicity of the dose-effect curve. The combination index (CI) for drug combinations is derived according to the equation below where n=number of drugs.

$$CI = \sum_{j=1}^{n} \frac{(f_a)_j}{(f_u)_j}$$

A log(CI) = 0 indicates an additive effect, a log(CI) < 0 indicates synergy, and a log(CI) > 0 indicates antagonism. The above median effect equation and CI allow a plot of CI values at different effect levels (fa's) are then determined by the CalcuSyn software (Biosoft).

5-12. Cell apoptosis assay

After indicated treatment, cells were harvested and processed according to the manufacture's protocol. Apoptotic cells were analyzed with LSRII (BD Biosciences) using the Annexin V FITC Apoptosis Detection Kit I (Fisher). The kit contains recombinant annexin V conjugated to fluorescein (FITC annexin V), as well as a ready-to-use solution of the red-fluorescent propidium iodide (PI) nucleic acid binding dye. It is based on the binding of fluorescently labeled Annexin V to phosphatidylserine and the permeation of 7-AAD to late-stage apoptotic and dead cells. PI is impermeant to live cells and apoptotic cells, but stains dead cells with red fluorescence, binding tightly to the nucleic acids in the cell. After staining a cell population with FITC annexin V and PI, apoptotic populations can easily be distinguished using a flow cytometer.

5-13. 3D cell culture

For 3-dimensional culture, 500 cells were seeded in 500ul media using a Cell Carrier Spheroid ULA 96-well Microplate (Perkin Elmer). Right after cell transfer, microplate centrifuged at 500g for 5min to force them to aggregate. Twenty-four hours after centrifugation, almost of cells formed spheres in the plate. Then, another 500ul of media with indicated drugs added to the well.

5-14. Small Animal Radiation Research Platform (SARRP)

The SARRP by Xstrahl (Camberley, Surrey, UK) was used to deliver radiation. Mice were anesthetized with isoflurane, an inhalational agent. The mice underwent computed tomographic (CT) imaging on the SARRP and deliver 1-2 Gy radiation in a 3-mm beam centered on the tumor as described in references.[113,114]

5-15. Chromatin accessibility

Cells were transfected with AAVS1 specific CRISPR/Cas9 using Lipofectamine 3000. After eight hours later, cells were harvested and processed according to the manufacturer's instructions (EpiQuick Chromatin Accessibility Kit, Epigentek). Quantification of chromatin accessibility by qPCR was performed with positive and negative controls designed for open and closed chromatin regions, respectively. Chromatin accessibility (%) (Fold enrichment) was assessed using the following calculation: $FE=2^{(Nse\ CT-no\text{-}Nse\ CT)}\times 100$ (Nse = Nuclease mix). Sequences used for pPCR near DSB sites (1~5 regions) and GAPDH are followed. (**Table 5-1**)

5-16. ATAC-Sequencing

ATAC-seq libraries were constructed by adapting a published protocol[115] by using Nextera DNA Library Preparation Kit (Illumina). Briefly, 50,000 cells were collected after with or without irradiation (3Gy), washed with cold PBS and resuspended in 50 μl of ES buffer (10μmM Tris pH 7.4, 10μmM NaCl, 3μmM MgCl2). Permeabilized cells were resuspended in 50 μl Transposase reaction (1X Tagmentation buffer, 1.0–1.5 μl Tn5 transposase enzyme) and incubated for 30min at 37°C. Subsequent steps of the protocol were performed as described in previous reference. [115]

5-17. Analyzing DSB junction

Cells (hEM and MCF10A) were transfected with AAVS1-specific CRISPR/Cas9 nucleases or with AAVS1-specific TALEN (HCT116). After 24 hours (CRISPR/Cas9) or 3 days (TALEN), genomic DNA was extracted and AAVS1 region was amplified by PCR using specific primers (**Table 5-2**). The amplified PCR products were sequenced followed by TOPO TA cloning (Invitrogen). All insertions or deletions from ARID1A wildtype and deficient cells was analyzed. CRISPR/Cas9 and TALEN (Left and Right arms) plasmids are kindly supported from Dr. Sonia Franco.

Primers	Sequence 5' to 3'
AAVS-#1-Forward	GGGTCACCTCTCACTCCTTTC
AAVS-#1-Reverse	CTGGAAGATGCCATGACAGG
AAVS-#2-Forward	GGGTCACCTCTCACTCCTTTC
AAVS-#2-Reverse	CGGGTTGGAGGAAGAAGACT
AAVS-#3-Forward	CCCCTATGTCCACTTCAGGA
AAVS-#3-Reverse	GGGTGGAGGGGACAGATAAA
AAVS-#4-Forward	CTCTTCCAGCCCCCTGTC
AAVS-#4-Reverse	AGCAAACATGCTGTCCTGAA
AAVS-#5-Forward	CCACCTCCTGTTAGGCAGAT
AAVS-#5-Reverse	GCTCCATCGTAAGCAAACCT
GAPDH-Forward	ACGTAGCTCAGGCCTCAAGA
GAPDH-Reverse	GCGGGCTCAATTTATAGAAAC

Table 5-1. Primer sequences used for chromatin accessibility. Five regions near DSB

sites in AAVS1 were amplified by using these primers. GAPDH primer used for control.

Primers	Sequence 5' to 3'
AAVS-Forward	TTCGGGTCACCTCTCACTCC
AAVS-Reverse	GGCTCCATCGTAAGCAAACC

Table 5-2. Primer sequences for amplifying AAVS1 region for DNA sequencing.

References.

1   Bray, F., Loos, A. H., Tognazzo, S. & La Vecchia, C. Ovarian cancer in Europe: Cross-sectional trends in incidence and mortality in 28 countries, 1953-2000. *International journal of cancer* **113**, 977-990, doi:10.1002/ijc.20649 (2005).

2   Edwards, B. K. *et al.* Annual report to the nation on the status of cancer, 1975-2002, featuring population-based trends in cancer treatment. *Journal of the National Cancer Institute* **97**, 1407-1427, doi:10.1093/jnci/dji289 (2005).

3   Kurman, R. J. & Shih Ie, M. The Dualistic Model of Ovarian Carcinogenesis: Revisited, Revised, and Expanded. *The American journal of pathology* **186**, 733-747, doi:10.1016/j.ajpath.2015.11.011 (2016).

4   Salani, R. *et al.* Assessment of TP53 mutation using purified tissue samples of ovarian serous carcinomas reveals a higher mutation rate than previously reported and does not correlate with drug resistance. *International journal of gynecological cancer : official journal of the International Gynecological Cancer Society* **18**, 487-491, doi:10.1111/j.1525-1438.2007.01039.x (2008).

5   Vang, R., Shih Ie, M. & Kurman, R. J. Ovarian low-grade and high-grade serous carcinoma: pathogenesis, clinicopathologic and molecular biologic features, and diagnostic problems. *Advances in anatomic pathology* **16**, 267-282, doi:10.1097/PAP.0b013e3181b4fffa (2009).

6   Longacre, T. A., McKenney, J. K., Tazelaar, H. D., Kempson, R. L. & Hendrickson, M. R. Ovarian serous tumors of low malignant potential (borderline tumors): outcome-based study of 276 patients with long-term (> or =5-year) follow-up. *The American journal of surgical pathology* **29**, 707-723 (2005).

7   McMeekin, D. S., Burger, R. A., Manetta, A., DiSaia, P. & Berman, M. L. Endometrioid adenocarcinoma of the ovary and its relationship to endometriosis. *Gynecologic oncology* **59**, 81-86, doi:10.1006/gyno.1995.1271 (1995).

8   Modesitt, S. C., Tortolero-Luna, G., Robinson, J. B., Gershenson, D. M. & Wolf, J. K. Ovarian and extraovarian endometriosis-associated cancer. *Obstetrics and gynecology* **100**, 788-795 (2002).

9   Erzen, M., Rakar, S., Klancnik, B. & Syrjanen, K. Endometriosis-associated ovarian carcinoma (EAOC): an entity distinct from other ovarian carcinomas as suggested by a nested case-control study. *Gynecologic oncology* **83**, 100-108, doi:10.1006/gyno.2001.6382 (2001).

10   Sainz de la Cuesta, R. *et al.* Histologic transformation of benign endometriosis to early epithelial ovarian cancer. *Gynecologic oncology* **60**, 238-244 (1996).

11   Wiegand, K. C. *et al.* ARID1A mutations in endometriosis-associated ovarian carcinomas. *The New England journal of medicine* **363**, 1532-1543, doi:10.1056/NEJMoa1008433 (2010).

12   Jones, S. *et al.* Frequent mutations of chromatin remodeling gene ARID1A in ovarian clear cell carcinoma. *Science (New York, N.Y.)* **330**, 228-231, doi:10.1126/science.1196333 (2010).

13   Kuo, K. T. *et al.* Frequent activating mutations of PIK3CA in ovarian clear cell carcinoma. *The American journal of pathology* **174**, 1597-1601, doi:10.2353/ajpath.2009.081000 (2009).

14   Yamamoto, S. *et al.* PIK3CA mutation is an early event in the development of endometriosis-associated ovarian clear cell adenocarcinoma. *The Journal of pathology* **225**, 189-194, doi:10.1002/path.2940 (2011).

15   Sugiyama, T. *et al.* Clinical characteristics of clear cell carcinoma of the ovary: a distinct histologic type with poor prognosis and resistance to platinum-based chemotherapy. *Cancer* **88**, 2584-2589 (2000).

16   Takano, M. *et al.* Clear cell carcinoma of the ovary: a retrospective multicentre experience of 254 patients with complete surgical staging. *British journal of cancer* **94**, 1369-1374, doi:10.1038/sj.bjc.6603116 (2006).

17   Kobayashi, H. *et al.* The role of hepatocyte nuclear factor-1beta in the pathogenesis of clear cell carcinoma of the ovary. *International journal of gynecological cancer : official journal of the*

International Gynecological Cancer Society **19**, 471-479, doi:10.1111/IGC.0b013e3181a19eca (2009).

18   Society, A. C. Cancer Facts and Figures 2016. (2016).

19   Bokhman, J. V. Two pathogenetic types of endometrial carcinoma. *Gynecologic oncology* **15**, 10-17 (1983).

20   Kandoth, C. *et al.* Integrated genomic characterization of endometrial carcinoma. *Nature* **497**, 67-73, doi:10.1038/nature12113 (2013).

21   Bosse, T. *et al.* Loss of ARID1A expression and its relationship with PI3K-Akt pathway alterations, TP53 and microsatellite instability in endometrial cancer. *Modern pathology : an official journal of the United States and Canadian Academy of Pathology, Inc* **26**, 1525-1535, doi:10.1038/modpathol.2013.96 (2013).

22   Banerjee, S. & Kaye, S. B. New strategies in the treatment of ovarian cancer: current clinical perspectives and future potential. *Clinical cancer research : an official journal of the American Association for Cancer Research* **19**, 961-968, doi:10.1158/1078-0432.ccr-12-2243 (2013).

23   Hollis, R. L. & Gourley, C. Genetic and molecular changes in ovarian cancer. *Cancer biology & medicine* **13**, 236-247, doi:10.20892/j.issn.2095-3941.2016.0024 (2016).

24   Neigeborn, L. & Carlson, M. Genes affecting the regulation of SUC2 gene expression by glucose repression in Saccharomyces cerevisiae. *Genetics* **108**, 845-858 (1984).

25   Stern, M., Jensen, R. & Herskowitz, I. Five SWI genes are required for expression of the HO gene in yeast. *Journal of molecular biology* **178**, 853-868 (1984).

26   Saha, A., Wittmeyer, J. & Cairns, B. R. Chromatin remodelling: the industrial revolution of DNA around histones. *Nature reviews. Molecular cell biology* **7**, 437-447, doi:10.1038/nrm1945 (2006).

27   Clapier, C. R. & Cairns, B. R. The biology of chromatin remodeling complexes. *Annual review of biochemistry* **78**, 273-304, doi:10.1146/annurev.biochem.77.062706.153223 (2009).

28   Garraway, L. A. & Lander, E. S. Lessons from the cancer genome. *Cell* **153**, 17-37, doi:10.1016/j.cell.2013.03.002 (2013).

29   Kadoch, C. *et al.* Proteomic and bioinformatic analysis of mammalian SWI/SNF complexes identifies extensive roles in human malignancy. *Nature genetics* **45**, 592-601, doi:10.1038/ng.2628 (2013).

30   Wu, R. C., Wang, T. L. & Shih Ie, M. The emerging roles of ARID1A in tumor suppression. *Cancer biology & therapy* **15**, 655-664, doi:10.4161/cbt.28411 (2014).

31   Bagchi, A. & Mills, A. A. The quest for the 1p36 tumor suppressor. *Cancer research* **68**, 2551-2556, doi:10.1158/0008-5472.can-07-2095 (2008).

32   Wang, K. *et al.* Exome sequencing identifies frequent mutation of ARID1A in molecular subtypes of gastric cancer. *Nature genetics* **43**, 1219-1223, doi:10.1038/ng.982 (2011).

33   Jones, S. *et al.* Somatic mutations in the chromatin remodeling gene ARID1A occur in several tumor types. *Human mutation* **33**, 100-103, doi:10.1002/humu.21633 (2012).

34   Zang, Z. J. *et al.* Exome sequencing of gastric adenocarcinoma identifies recurrent somatic mutations in cell adhesion and chromatin remodeling genes. *Nature genetics* **44**, 570-574, doi:10.1038/ng.2246 (2012).

35   Wang, X. *et al.* Expression of p270 (ARID1A), a component of human SWI/SNF complexes, in human tumors. *International journal of cancer* **112**, 636, doi:10.1002/ijc.20450 (2004).

36   Streppel, M. M. *et al.* Next-generation sequencing of endoscopic biopsies identifies ARID1A as a tumor-suppressor gene in Barrett's esophagus. *Oncogene* **33**, 347-357, doi:10.1038/onc.2012.586 (2014).

37   Dulak, A. M. *et al.* Exome and whole-genome sequencing of esophageal adenocarcinoma identifies recurrent driver events and mutational complexity. *Nature genetics* **45**, 478-486, doi:10.1038/ng.2591 (2013).

38   Huang, J., Zhao, Y. L., Li, Y., Fletcher, J. A. & Xiao, S. Genomic and functional evidence for an ARID1A tumor suppressor role. *Genes, chromosomes & cancer* **46**, 745-750, doi:10.1002/gcc.20459 (2007).

39   Treon, S. P. *et al.* MYD88 L265P somatic mutation in Waldenstrom's macroglobulinemia. *The New England journal of medicine* **367**, 826-833, doi:10.1056/NEJMoa1200710 (2012).

40   Giulino-Roth, L. *et al.* Targeted genomic sequencing of pediatric Burkitt lymphoma identifies recurrent alterations in antiapoptotic and chromatin-remodeling genes. *Blood* **120**, 5181-5184, doi:10.1182/blood-2012-06-437624 (2012).

41   Guichard, C. *et al.* Integrated analysis of somatic mutations and focal copy-number changes identifies key genes and pathways in hepatocellular carcinoma. *Nature genetics* **44**, 694-698, doi:10.1038/ng.2256 (2012).

42   Fujimoto, A. *et al.* Whole-genome sequencing of liver cancers identifies etiological influences on mutation patterns and recurrent mutations in chromatin regulators. *Nature genetics* **44**, 760-764, doi:10.1038/ng.2291 (2012).

43   Chan-On, W. *et al.* Exome sequencing identifies distinct mutational patterns in liver fluke-related and non-infection-related bile duct cancers. *Nature genetics* **45**, 1474-1478, doi:10.1038/ng.2806 (2013).

44   Jiao, Y. *et al.* Exome sequencing identifies frequent inactivating mutations in BAP1, ARID1A and PBRM1 in intrahepatic cholangiocarcinomas. *Nature genetics* **45**, 1470-1473, doi:10.1038/ng.2813 (2013).

45   Guo, G. *et al.* Whole-genome and whole-exome sequencing of bladder cancer identifies frequent alterations in genes involved in sister chromatid cohesion and segregation. *Nature genetics* **45**, 1459-1463, doi:10.1038/ng.2798 (2013).

46   Gui, Y. *et al.* Frequent mutations of chromatin remodeling genes in transitional cell carcinoma of the bladder. *Nature genetics* **43**, 875-878, doi:10.1038/ng.907 (2011).

47   Balbas-Martinez, C. *et al.* ARID1A alterations are associated with FGFR3-wild type, poor-prognosis, urothelial bladder tumors. *PloS one* **8**, e62483, doi:10.1371/journal.pone.0062483 (2013).

48   Guan, B. *et al.* Mutation and loss of expression of ARID1A in uterine low-grade endometrioid carcinoma. *The American journal of surgical pathology* **35**, 625-632, doi:10.1097/PAS.0b013e318212782a (2011).

49   Guan, B. *et al.* Roles of deletion of Arid1a, a tumor suppressor, in mouse ovarian tumorigenesis. *Journal of the National Cancer Institute* **106**, doi:10.1093/jnci/dju146 (2014).

50   Yamamoto, S., Tsuda, H., Takano, M., Tamai, S. & Matsubara, O. Loss of ARID1A protein expression occurs as an early event in ovarian clear-cell carcinoma development and frequently coexists with PIK3CA mutations. *Modern pathology : an official journal of the United States and Canadian Academy of Pathology, Inc* **25**, 615-624, doi:10.1038/modpathol.2011.189 (2012).

51   Huang, H. N., Lin, M. C., Huang, W. C., Chiang, Y. C. & Kuo, K. T. Loss of ARID1A expression and its relationship with PI3K-Akt pathway alterations and ZNF217 amplification in ovarian clear cell carcinoma. *Modern pathology : an official journal of the United States and Canadian Academy of Pathology, Inc* **27**, 983-990, doi:10.1038/modpathol.2013.216 (2014).

52   Guan, B., Wang, T. L. & Shih Ie, M. ARID1A, a factor that promotes formation of SWI/SNF-mediated chromatin remodeling, is a tumor suppressor in gynecologic cancers. *Cancer research* **71**, 6718-6727, doi:10.1158/0008-5472.can-11-1562 (2011).

53   Wu, R. C. *et al.* Frequent somatic mutations of the telomerase reverse transcriptase promoter in ovarian clear cell carcinoma but not in other major types of gynaecological malignancy. *The Journal of pathology* **232**, 473-481, doi:10.1002/path.4315 (2014).

54   Suryo Rahmanto, Y. *et al.* Inactivating ARID1A Tumor Suppressor Enhances TERT Transcription and Maintains Telomere Length in Cancer Cells. *The Journal of biological chemistry* **291**, 9690-9699, doi:10.1074/jbc.M115.707612 (2016).

55   Caldecott, K. W. DNA single-strand break repair. *Experimental cell research* **329**, 2-8, doi:10.1016/j.yexcr.2014.08.027 (2014).

56   Ciccia, A. & Elledge, S. J. The DNA damage response: making it safe to play with knives. *Molecular cell* **40**, 179-204, doi:10.1016/j.molcel.2010.09.019 (2010).

57   Jiricny, J. The multifaceted mismatch-repair system. *Nature reviews. Molecular cell biology* **7**, 335-346, doi:10.1038/nrm1907 (2006).

58   Cerrato, A., Morra, F. & Celetti, A. Use of poly ADP-ribose polymerase [PARP] inhibitors in cancer cells bearing DDR defects: the rationale for their inclusion in the clinic. *Journal of experimental & clinical cancer research : CR* **35**, 179, doi:10.1186/s13046-016-0456-2 (2016).

59   Song, J., Keppler, B. D., Wise, R. R. & Bent, A. F. PARP2 Is the Predominant Poly(ADP-Ribose) Polymerase in Arabidopsis DNA Damage and Immune Responses. *PLoS genetics* **11**, e1005200, doi:10.1371/journal.pgen.1005200 (2015).

60   Mladenov, E., Magin, S., Soni, A. & Iliakis, G. DNA double-strand break repair as determinant of cellular radiosensitivity to killing and target in radiation therapy. *Frontiers in oncology* **3**, 113, doi:10.3389/fonc.2013.00113 (2013).

61   Onn, I., Heidinger-Pauli, J. M., Guacci, V., Unal, E. & Koshland, D. E. Sister chromatid cohesion: a simple concept with a complex reality. *Annual review of cell and developmental biology* **24**, 105-129, doi:10.1146/annurev.cellbio.24.110707.175350 (2008).

62   San Filippo, J., Sung, P. & Klein, H. Mechanism of eukaryotic homologous recombination. *Annual review of biochemistry* **77**, 229-257, doi:10.1146/annurev.biochem.77.061306.125255 (2008).

63   Lieber, M. R. The mechanism of double-strand DNA break repair by the nonhomologous DNA end-joining pathway. *Annual review of biochemistry* **79**, 181-211, doi:10.1146/annurev.biochem.052308.093131 (2010).

64   Helleday, T., Lo, J., van Gent, D. C. & Engelward, B. P. DNA double-strand break repair: from mechanistic understanding to cancer treatment. *DNA repair* **6**, 923-935, doi:10.1016/j.dnarep.2007.02.006 (2007).

65   Ball, A. R., Jr. & Yokomori, K. Damage site chromatin: open or closed? *Current opinion in cell biology* **23**, 277-283, doi:10.1016/j.ceb.2011.03.012 (2011).

66   Aydin, O. Z., Vermeulen, W. & Lans, H. ISWI chromatin remodeling complexes in the DNA damage response. *Cell cycle (Georgetown, Tex.)* **13**, 3016-3025, doi:10.4161/15384101.2014.956551 (2014).

67   Downs, J. A., Lowndes, N. F. & Jackson, S. P. A role for Saccharomyces cerevisiae histone H2A in DNA repair. *Nature* **408**, 1001-1004, doi:10.1038/35050000 (2000).

68   Kruhlak, M. J. *et al.* Changes in chromatin structure and mobility in living cells at sites of DNA double-strand breaks. *The Journal of cell biology* **172**, 823-834, doi:10.1083/jcb.200510015 (2006).

69   Morrison, A. J. *et al.* INO80 and gamma-H2AX interaction links ATP-dependent chromatin remodeling to DNA damage repair. *Cell* **119**, 767-775, doi:10.1016/j.cell.2004.11.037 (2004).

70   van Attikum, H., Fritsch, O., Hohn, B. & Gasser, S. M. Recruitment of the INO80 complex by H2A phosphorylation links ATP-dependent chromatin remodeling with DNA double-strand break repair. *Cell* **119**, 777-788, doi:10.1016/j.cell.2004.11.033 (2004).

71   Kusch, T. *et al.* Acetylation by Tip60 is required for selective histone variant exchange at DNA lesions. *Science (New York, N.Y.)* **306**, 2084-2087, doi:10.1126/science.1103455 (2004).

72   Tsukuda, T., Fleming, A. B., Nickoloff, J. A. & Osley, M. A. Chromatin remodelling at a DNA double-strand break site in Saccharomyces cerevisiae. *Nature* **438**, 379-383, doi:10.1038/nature04148 (2005).

73   Downs, J. A. *et al.* Binding of chromatin-modifying activities to phosphorylated histone H2A at DNA damage sites. *Molecular cell* **16**, 979-990, doi:10.1016/j.molcel.2004.12.003 (2004).

74   Gong, F., Fahy, D., Liu, H., Wang, W. & Smerdon, M. J. Role of the mammalian SWI/SNF chromatin remodeling complex in the cellular response to UV damage. *Cell cycle (Georgetown, Tex.)* **7**, 1067-1074, doi:10.4161/cc.7.8.5647 (2008).

75   Zhang, L., Zhang, Q., Jones, K., Patel, M. & Gong, F. The chromatin remodeling factor BRG1 stimulates nucleotide excision repair by facilitating recruitment of XPC to sites of DNA damage. *Cell cycle (Georgetown, Tex.)* **8**, 3953-3959, doi:10.4161/cc.8.23.10115 (2009).

76   Zhao, Q. *et al.* Modulation of nucleotide excision repair by mammalian SWI/SNF chromatin-remodeling complex. *The Journal of biological chemistry* **284**, 30424-30432, doi:10.1074/jbc.M109.044982 (2009).

77   Klochendler-Yeivin, A., Picarsky, E. & Yaniv, M. Increased DNA damage sensitivity and apoptosis in cells lacking the Snf5/Ini1 subunit of the SWI/SNF chromatin remodeling complex. *Molecular and cellular biology* **26**, 2661-2674, doi:10.1128/mcb.26.7.2661-2674.2006 (2006).

78   Watanabe, R. *et al.* SWI/SNF factors required for cellular resistance to DNA damage include ARID1A and ARID1B and show interdependent protein stability. *Cancer research* **74**, 2465-2475, doi:10.1158/0008-5472.can-13-3608 (2014).

79   Bitler, B. G. *et al.* Synthetic lethality by targeting EZH2 methyltransferase activity in ARID1A-mutated cancers. *Nature medicine* **21**, 231-238, doi:10.1038/nm.3799 (2015).

80   Shen, J. *et al.* ARID1A Deficiency Impairs the DNA Damage Checkpoint and Sensitizes Cells to PARP Inhibitors. *Cancer discovery* **5**, 752-767, doi:10.1158/2159-8290.cd-14-0849 (2015).

81   Negrini, S., Gorgoulis, V. G. & Halazonetis, T. D. Genomic instability--an evolving hallmark of cancer. *Nature reviews. Molecular cell biology* **11**, 220-228, doi:10.1038/nrm2858 (2010).

82   Dietlein, F. & Reinhardt, H. C. Molecular pathways: exploiting tumor-specific molecular defects in DNA repair pathways for precision cancer therapy. *Clinical cancer research : an official journal of the American Association for Cancer Research* **20**, 5882-5887, doi:10.1158/1078-0432.ccr-14-1165 (2014).

83   Reinhardt, H. C., Jiang, H., Hemann, M. T. & Yaffe, M. B. Exploiting synthetic lethal interactions for targeted cancer therapy. *Cell cycle (Georgetown, Tex.)* **8**, 3112-3119, doi:10.4161/cc.8.19.9626 (2009).

84   Ciriello, G. *et al.* Emerging landscape of oncogenic signatures across human cancers. *Nature genetics* **45**, 1127-1133, doi:10.1038/ng.2762 (2013).

85   Hanks, S. *et al.* Constitutional aneuploidy and cancer predisposition caused by biallelic mutations in BUB1B. *Nature genetics* **36**, 1159-1161, doi:10.1038/ng1449 (2004).

86   Hanahan, D. & Weinberg, R. A. Hallmarks of cancer: the next generation. *Cell* **144**, 646-674, doi:10.1016/j.cell.2011.02.013 (2011).

87   Curtin, N. J. DNA repair dysregulation from cancer driver to therapeutic target. *Nature reviews. Cancer* **12**, 801-817, doi:10.1038/nrc3399 (2012).

88   Wang, C. & Lees-Miller, S. P. Detection and repair of ionizing radiation-induced DNA double strand breaks: new developments in nonhomologous end joining. *International journal of radiation oncology, biology, physics* **86**, 440-449, doi:10.1016/j.ijrobp.2013.01.011 (2013).

89   Taccioli, G. E. *et al.* Targeted disruption of the catalytic subunit of the DNA-PK gene in mice confers severe combined immunodeficiency and radiosensitivity. *Immunity* **9**, 355-366 (1998).

90   Rosenzweig, K. E., Youmell, M. B., Palayoor, S. T. & Price, B. D. Radiosensitization of human tumor cells by the phosphatidylinositol3-kinase inhibitors wortmannin and LY294002 correlates with inhibition of DNA-dependent protein kinase and prolonged G2-M delay. *Clinical cancer research : an official journal of the American Association for Cancer Research* **3**, 1149-1156 (1997).

91   Veuger, S. J., Curtin, N. J., Richardson, C. J., Smith, G. C. & Durkacz, B. W. Radiosensitization and DNA repair inhibition by the combined use of novel inhibitors of DNA-dependent protein kinase and poly(ADP-ribose) polymerase-1. *Cancer research* **63**, 6008-6015 (2003).

92   Ciszewski, W. M., Tavecchio, M., Dastych, J. & Curtin, N. J. DNA-PK inhibition by NU7441 sensitizes breast cancer cells to ionizing radiation and doxorubicin. *Breast cancer research and treatment* **143**, 47-55, doi:10.1007/s10549-013-2785-6 (2014).

93   Ernestos, B. *et al.* Increased chromosomal radiosensitivity in women carrying BRCA1/BRCA2 mutations assessed with the G2 assay. *International journal of radiation oncology, biology, physics* **76**, 1199-1205, doi:10.1016/j.ijrobp.2009.10.020 (2010).

94   Kuhne, M. *et al.* A double-strand break repair defect in ATM-deficient cells contributes to radiosensitivity. *Cancer research* **64**, 500-508 (2004).

95   Wang, H., Wang, H., Powell, S. N., Iliakis, G. & Wang, Y. ATR affecting cell radiosensitivity is dependent on homologous recombination repair but independent of nonhomologous end joining. *Cancer research* **64**, 7139-7143, doi:10.1158/0008-5472.can-04-1289 (2004).

96   Zhou, Z. R. *et al.* The Chk1 inhibitor MK-8776 increases the radiosensitivity of human triple-negative breast cancer by inhibiting autophagy. *Acta pharmacologica Sinica* **38**, 513-523, doi:10.1038/aps.2016.136 (2017).

97   Senra, J. M. *et al.* Inhibition of PARP-1 by olaparib (AZD2281) increases the radiosensitivity of a lung tumor xenograft. *Molecular cancer therapeutics* **10**, 1949-1958, doi:10.1158/1535-7163.mct-11-0278 (2011).

98   Kaelin, W. G., Jr. The concept of synthetic lethality in the context of anticancer therapy. *Nature reviews. Cancer* **5**, 689-698, doi:10.1038/nrc1691 (2005).

99   Nijman, S. M. & Friend, S. H. Cancer. Potential of the synthetic lethality principle. *Science (New York, N.Y.)* **342**, 809-811, doi:10.1126/science.1244669 (2013).

100   Farmer, H. *et al.* Targeting the DNA repair defect in BRCA mutant cells as a therapeutic strategy. *Nature* **434**, 917-921, doi:10.1038/nature03445 (2005).

101   Fong, P. C. *et al.* Inhibition of poly(ADP-ribose) polymerase in tumors from BRCA mutation carriers. *The New England journal of medicine* **361**, 123-134, doi:10.1056/NEJMoa0900212 (2009).

102   Bryant, H. E. *et al.* Specific killing of BRCA2-deficient tumours with inhibitors of poly(ADP-ribose) polymerase. *Nature* **434**, 913-917, doi:10.1038/nature03443 (2005).

103   Pommier, Y., O'Connor, M. J. & de Bono, J. Laying a trap to kill cancer cells: PARP inhibitors and their mechanisms of action. *Science translational medicine* **8**, 362ps317, doi:10.1126/scitranslmed.aaf9246 (2016).

104   De Lorenzo, S. B., Patel, A. G., Hurley, R. M. & Kaufmann, S. H. The Elephant and the Blind Men: Making Sense of PARP Inhibitors in Homologous Recombination Deficient Tumor Cells. *Frontiers in oncology* **3**, 228, doi:10.3389/fonc.2013.00228 (2013).

105   Dietlein, F., Thelen, L. & Reinhardt, H. C. Cancer-specific defects in DNA repair pathways as targets for personalized therapeutic approaches. *Trends in genetics : TIG* **30**, 326-339, doi:10.1016/j.tig.2014.06.003 (2014).

106   Murai, J. *et al.* Trapping of PARP1 and PARP2 by Clinical PARP Inhibitors. *Cancer research* **72**, 5588-5599, doi:10.1158/0008-5472.can-12-2753 (2012).

107   Murai, J. *et al.* Stereospecific PARP trapping by BMN 673 and comparison with olaparib and rucaparib. *Molecular cancer therapeutics* **13**, 433-443, doi:10.1158/1535-7163.mct-13-0803 (2014).

108   Ziv, Y. *et al.* Chromatin relaxation in response to DNA double-strand breaks is modulated by a novel ATM- and KAP-1 dependent pathway. *Nature cell biology* **8**, 870-876, doi:10.1038/ncb1446 (2006).

109   Certo, M. T. *et al.* Tracking genome engineering outcome at individual DNA breakpoints. *Nature methods* **8**, 671-676, doi:10.1038/nmeth.1648 (2011).

110   Lee, L. J., Bu, P., Feltmate, C. & Viswanathan, A. N. Adjuvant chemotherapy with external beamradiation therapy for high-grade, node-positive endometrial cancer. *International journal of gynecological cancer : official journal of the International Gynecological Cancer Society* **24**, 1441-1448, doi:10.1097/igc.0000000000000248 (2014).

111   Ahel, D. *et al.* Poly(ADP-ribose)-dependent regulation of DNA repair by the chromatin remodeling enzyme ALC1. *Science (New York, N.Y.)* **325**, 1240-1243, doi:10.1126/science.1177321 (2009).

112   Perets, R. *et al.* Transformation of the fallopian tube secretory epithelium leads to high-grade serous ovarian cancer in Brca;Tp53;Pten models. *Cancer cell* **24**, 751-765, doi:10.1016/j.ccr.2013.10.013 (2013).

113   Zeng, J. *et al.* Anti-PD-1 blockade and stereotactic radiation produce long-term survival in mice with intracranial gliomas. *International journal of radiation oncology, biology, physics* **86**, 343-349, doi:10.1016/j.ijrobp.2012.12.025 (2013).

114   Wong, J. *et al.* High-resolution, small animal radiation research platform with x-ray tomographic guidance capabilities. *International journal of radiation oncology, biology, physics* **71**, 1591-1599, doi:10.1016/j.ijrobp.2008.04.025 (2008).

115   Buenrostro, J. D., Wu, B., Chang, H. Y. & Greenleaf, W. J. ATAC-seq: A Method for Assaying Chromatin Accessibility Genome-Wide. *Current protocols in molecular biology* **109**, 21.29.21-29, doi:10.1002/0471142727.mb2129s109 (2015).

Curriculum Vitae

Youngran Park

Ph.D. Candidate   Phone: (917) 488-2786
Pathobiology Program   e-mail: youngran.park35@gmail.com or
Department of Pathology   ypark36@jhmi.edu
Johns Hopkins University   3942 Cloverhill Rd
School of Medicine   Baltimore MD, 21218

EDUCATION

2017.9	–	**Ph.D.** Candidate, Pathobiology Program
2011.8		Johns Hopkins University, School of Medicine
		Advisors: Ie-Ming Shih M.D, Ph.D., Tian-Li Wang Ph.D.
2010.2	–	**B.S.** Biotechnology, College of Life Sciences
2005.3		Seoul, Korea University

PUBLICATIONS

Youngran Park*, et al., The Caretaker Role of ARID1A in DNA Repair and the Effects of Targeted Therapy in ARID1A Mutated Cancers (In manuscript preparation)

Suryo Rahmanto* Y, Shen W, Shi X, Yu Y, Chen X, Lee M-H, Vitolo MI, **Youngran Park**, Bahadirli-Talbott A, Miyamoto T, Wirtz D, Martin SS, Drapkin D, Xuan J, Shih IM, Wang TL. Inactivation of ARID1A-SWI/SNF complex alters chromatin compactness at enhancer regions and affects transcription of key tumor signaling circuitry (In manuscript preparation)

Mi Kyung Park*, **Youngran Park***, Jaegal Shim*, et al., Novel involvement of leukotriene B4 receptor 2 through ERK activation by PP2A down-regulation in leukotriene B4-induced keratin phosphorylation and reorganization of pancreatic cancer cells, Biochimica et Biophysica Acta, 1823 (2012) 2120–2129

RESEARCH EXPERIENCES

Johns Hopkins University School of Medicine 2011 – 2017

Ph.D. Thesis advisors: Ie-Ming Shih MD, Ph.D., Tian-Li Wang Ph.D.

- Thesis Project : The Caretaker Role of ARID1A in DNA Repair and the Effects of Targeted Therapy in ARID1A Mutated Cancers

Cancer Experimental Resources Branch of National Cancer Center(NCC), Korea, 2010 - 2011

Researcher, Certified by Jin Soo Lee (M.D., Ph.D., President of NCC)
Co-advisor : Chang Hoon Lee (Ph.D., Prof. of Dongguk Univ.), Ho Lee (Ph.D., PI of NCC)

- Project 1 : Cancer Metastasis via Keratin Reorganization
Researching on the Inflammatory mediator-induced keratin reorganization and migration

- Project 2 : Producing EMP2 gene Knock-out (KO) mice
Participating in KO mice production by preparing embryos and performing
subsequent manipulation

Molecular Oncology Branch of National Cancer Center, Korea, 2009

Intern Researcher, Summer Undergraduate Research Fellowship (SURF)
Advisor : Soo Youl Kim (Ph.D., PI of NCC)

- Project : Development of monoclonal Transglutaminase-2 antibodies

Medtronics Department of the Europe branch of Korea Institute Science and Technology (KIST-Europe), Germany, 2008 - 2009

Intern Researcher, Certified by Chang Ho Kim (Dr. Institute Director of KIST-Europe)
Advisor : Ute Shteinfeld (Ph.D., Group leader), Anja Philippi (Ph.D., Team leader)

- Project : Development of drug delivery system by using human T lymphocytes
Performing cell viability tests and experiments with confocal microscope

TRANSLATIONAL ROTATIONS

Pediatric Oncology Clinic, Johns Hopkins Hospital, 2017, April – May
  Advisor : Eric Hutton Raabe, M.D., Ph.D
  - Learn about multidisciplinary clinic in pediatric oncology outpatient and inpatient

Molecular Diagnostics Lab, Johns Hopkins Hospital, 2016, April
  Advisor : James Richard Eshleman, Jr, M.D., Ph.D.
  - Learn about molecular diagnostics technologies available to researchers
  : Capillary electrophoresis, Pyro sequencing, Next generation sequencing

TALKS

Youngran Park, Ie-Ming Shih, Tian-Li Wang. Enhancing the Cytotoxic Effects of Radiation with PARP inhibitors in ARID1A Mutated Neoplasms, Pathology Grand Round, Baltimore, 2017, May, 22

Youngran Park, Ie-Ming Shih, Tian-Li Wang. Precision Medicine by Applying Radiation Therapy and PARP Inhibitor in ARID1A Mutated Neoplasm, Chromatin & Chromosomes Workshop, Baltimore, 2017, May, 8

Youngran Park, Ie-Ming Shih, Tian-Li Wang. The Role of ARID1A in DNA Damage Repair, Annual Pathobiology Program Retreat, Baltimore, 2016, September, 9

POSTER PRESENTATIONS

Youngran Park, Ie-Ming Shih, Tian-Li Wang. Enhancing the Cytotoxic Effects of Radiation with PARP inhibitors in ARID1A Mutated Neoplasms, Sidney Kimmel Comprehensive Cancer Center Fellow Research Day, Baltimore, 2017

Youngran Park, Ie-Ming Shih, Tian-Li Wang. Precision Medicine by Applying Radiation Therapy and PARP Inhibitor in ARID1A Mutated Neoplasm, Chromatin & Chromosomes Workshop, Baltimore, 2017

Youngran Park, Ie-Ming Shih, Tian-Li Wang. Precision Medicine by Applying Radiation Therapy and PARP Inhibitor in ARID1A Mutated Neoplasms, Sidney Kimmel Comprehensive Cancer Center Fellow Research Day, Baltimore, 2017

Youngran Park, Ie-Ming Shih, Tian-Li Wang. Precision Medicine by Applying Radiation Therapy and PARP Inhibitor in ARID1A Mutated Neoplasms, Pathology Young Investigator's Day, Baltimore, 2017

Youngran Park, Ie-Ming Shih, Tian-Li Wang. ARID1A Promotes Double Strand Breaks Repair in Gynecological Cancer, Sidney Kimmel Comprehensive Cancer Center Fellow Research Day, Baltimore, 2016

Youngran Park, Ie-Ming Shih, Tian-Li Wang. ARID1A Promotes Double Strand Breaks Repair in Gynecological Cancer, Baltimore Area Repair Symposium, Baltimore, 2016

Youngran Park, Ie-Ming Shih, Tian-Li Wang. Precision Medicine by Applying Radiation Therapy and PARP Inhibitor in ARID1A Mutated Neoplasms, Pathology Young Investigator's Day, Baltimore, 2016

Youngran Park, Tian-Li Wang, Ie-Ming Shih, Annual Pathobiology Program Retreat (2011-present, annually)

Youngran Park, Yohan Suryo Rahmanto, Tae Mogami, Ie-Ming Shih and Tian-Li Wang, ARID1A promotes double strand breaks repair, Young Generation Technical and Leadership Conference, Orlando, 2014

Youngran Park, Yohan Suryo Rahmanto, Tae Mogami, Ie-Ming Shih and Tian-Li Wang, PI3K Inhibitor Sensitizes ARID1A-Mutated Human Cancers to DNA Damaging Agents, Members of a consortium funded by the US Department of Defense, 5th Annual Ovarian Cancer Symposium, Toronto, 2014

Youngran Park, Hyoung June Kim, Min Soo Noh, Kwang Mi Kim, Mi Kyung Park, Hye Ja Lee, Ho Lee and Chang Hoon Lee, Glucosylsphingosine Induces Itch-Scratch Responses in Mice. The Korean Society of Applied Pharmacology, Seoul National University, Korea, 2010

Youngran Park, Kang Seo Park, Soo Youl Kim, Development of monoclonal Transglutaminase-2 antibodies. National Cancer Center, Korea, 2009

TEACHING EXPERIENCES

2011 – 2017	Mentor for rotation students and undergraduate students, Johns Hopkins, USA
2014	Disease Mechanisms and Pathology, Johns Hopkins, USA
2010 - 2011	Mentor for rotation students and undergraduate students, National Cancer Center, Korea

HONORS & AWARDS

Pathology Young Investigator's Day Award (*two times*)	Offered to researcher with excellence in basic research by Johns Hopkins University, 2016, 2017 $500 each
Travel Grant	Graduate Student Association, Johns Hopkins University, 2015, $300
Mogam Scholarship	Offered to talented student in Science by Mogam Science Scholarship Foundation, 2012, $10,000
Margaret Lee Scholarship	Talented international students who applied for Ph.D. Program at Johns Hopkins University, 2011-2012, $74,893
Study Scholarships (*two times*)	Offered to students with good study performance by Korea University, 2006, 2009
Semester High Honors	Offered to student with good achievement by Korea University, 2007
Alumni Scholarships (*four times*)	Offered to student with good study performance by Korea University Alumni, 2006 – 2008
Honors Scholarships	Offered to the top 5 percent of students in each department by Korea University, 2005

REFERENCES

Ie-Ming Shih, MD, PhD

Richard W. TeLinde Professor
Department of Gynecology and Obstetrics
Departments of Pathology and Oncology
Faculty in Pathobiology Graduate Program
Johns Hopkins University
School of Medicine

Tian-Li Wang, PhD

Professor
Departments of Pathology and Oncology
Faculty in Pathobiology Graduate Program
Johns Hopkins University
School of Medicine

To me, the spirit of translational research is

to alleviate human suffering through research

and contribute to the equality.